JOURNAL OF GEOPHYSICAL RESEARCH, VOL. 95, NO. B7, PAGES 11,051–11,071, JULY 10, 1990

The Upper Mantle Degree 2: Constraints and Inferences From Global Mantle Wave Attenuation Measurements

BARBARA ROMANOWICZ

Laboratoire de Sismologie, Institut de Physique du Globe, Paris, France

We present the results of an analysis of global lateral variations in anelasticity of the upper mantle, as measured from very long period Rayleigh waves observed on the GEOSCOPE network. Four consecutive wave trains are used on each record to eliminate uncertainty on the amplitude at the source and to take into account, in a linear manner, focussing effects due to lateral variations in elastic parameters. Local estimates of attenuation are obtained using an inversion method based on the introduction of a correlation length, as an alternative to spherical harmonics expansion. Comparison of phase velocity and attenuation maps obtained at various periods shows a strong correlation of high-Q and high-velocity regions (respectively low Q and low velocity) both for great circle and minor arc data, at periods around 200 s. The detailed analysis of the degree 2 pattern, well resolved in the attenuation maps around this period, shows that it originates in the depth range 250–500 km and indicates that of the upper mantle degree 2 pattern observed in shear velocity is likely to be of thermal origin, possibly related to the topmost part of the large-scale convective system. Corrections for dispersion due to anelastic attenuation in degree 2 lead to significant decrease of corresponding lateral variations in shear velocity and a better agreement in phase and amplitude of the upper mantle degree 2 pattern with that observed in the geoid. This study shows that it is important to consider correcting presently available upper mantle tomographic models for the effects of intrinsic attenuation at long periods, before performing any comparison with short-period data or other geophysical parameters.

1. INTRODUCTION

Several global three-dimensional (3-D) models of upper mantle shear velocity structure have been obtained in recent years, based on the analysis of long-period surface waves from increasingly numerous digital stations [*Woodhouse and Dziewonski*, 1984; *Nataf et al.*, 1986; *Tanimoto*, 1986; *Montagner and Tanimoto*, 1990]. While these models differ in detail, they show several consistent features, in particular a strong correlation of the velocity distribution with surface tectonic features in the upper 250 km of the mantle and a dominant degree 2 pattern below that depth. This striking degree 2 pattern was first described in a study of fundamental spheroidal mode peak shifts by *Masters et al.* [1982], who interpreted it as originating in the upper mantle transition zone (400–670 km).

The 3-D studies of the upper mantle mentioned above gave us information on the elastic structure of the Earth and were all based on the assumption that the effect of lateral variations in anelastic attenuation, as measured by the quality factor Q, could be neglected, and a spherically symmetric preassigned Q model of the upper mantle was considered in the studies based on waveform inversion.

Yet evidence for lateral variations in Q in the upper mantle is abundant at long periods, both on a regional and on a global scale [e.g., *Canas and Mitchell*, 1978; *Lee and Solomon*, 1979; *Sipkin and Jordan*, 1980]. In the normal modes and mantle waves domain which interests us more specifically here, *Roult* [1982] measured particularly low Q for fundamental spheroidal modes on paths containing a large proportion of young oceans, and *Nakanishi* [1979*a*] regionalized long-period surface waves according to tectonic provinces and found evidence for significant variations from one province to another, as did *Mills and Hales* [1978]. More recently, *Dziewonski and Steim* [1982] also found significant differences between oceanic and continental Q in a global study of surface wave attenuation. Finally, large-scale lateral variations in the attenuation of fundamental spheroidal modes, correlated with local frequency variations, have been documented in our recent studies [*Romanowicz et al.*, 1987; *Roult et al.*, 1990].

While lateral variations in seismic velocities in the upper mantle are known not to exceed a few percent, measurements of attenuation, although much less accurate, indicate possible lateral variations of the order of 50–100%. It can therefore be expected that such large lateral variations in Q will introduce nonnegligible dispersion in the measured phase velocities or eigenfrequencies, which should be considered in the modelling process, just as they are now taken into account in average, spherically symmetric elastic models of Earth [e.g., *Anderson and Hart*, 1978; *Dziewonski and Anderson*, 1981]. This was, in fact, pointed out by *Nakanishi* [1979*b*], who remarked that the lateral variations in phase velocity were greatly reduced when dispersion due to lateral variations in anelasticity was considered, using the classical corrections for a model of intrinsic attenuation independent of frequency [e.g., *Liu et al.*, 1976; *Kanamori and Anderson*, 1977]. Measuring lateral variations in Q on a global scale is therefore of importance, not only because it can provide additional constraints on the thermal structure of the mantle, its viscosity, and its rheology but also because of its implications on the 3-D velocity structure.

However, measurement of attenuation is known to be difficult, also at long periods, since amplitudes of surface waves are strongly affected by lateral heterogeneity in velocity, which produces focussing and defocussing effects whose behavior can be quite nonlinear [e.g., *Lay and Kanamori*, 1985]. It is therefore a delicate problem to separate intrinsic attenuation effects from the effects of scattering and focussing. Some theoretical progress has been made in recent years in order to quantify better the contri-

Paper number 89JB03565.
0148-0227/90/89JB-03565$05.00

bution of focussing to the measured amplitudes. Using either a ray theoretical approach [*Woodhouse and Wong*, 1986; *Jobert*, 1986] or a normal mode approach [*Park*, 1987; *Romanowicz*, 1987], it has been shown that to first order, focussing effects can be described in terms of first and second transverse derivatives of the phase velocity along the great circle path joining epicenter and station. While this theory only describes linear effects, it is a valuable step toward understanding the perturbing effects in the amplitudes not due to intrinsic anelasticity, and more exact calculations of amplitudes in a laterally heterogeneous Earth can now also be performed using a theory that describes coupling of modes in an increasingly accurate manner [e.g., *Park*, 1987; *Smith and Masters*, 1989; *Tsuboi and Geller*, 1989; *Lognonné and Romanowicz*, 1990]. Therefore, as global high-quality digital long-period data become more numerous, it is now possible to try and determine lateral variations in long-period surface wave Q with better resolution and to examine their relation to the shear velocity models. In particular, no a priori assumptions about the correlation of the Q distribution with tectonic features need be assumed, a progress that was achieved much earlier for the 3-D velocity models of the upper mantle [e.g., *Woodhouse and Dziewonski*, 1984].

In this paper, we present results of a global study of mantle wave attenuation using data from the GEOSCOPE network [*Romanowicz et al.*, 1984]. This study is a follow up of our recent spheroidal mode free oscillation study [*Romanowicz et al.*, 1987; *Roult et al.*, 1990], and our first goal has been to seek confirmation of the degree 2 pattern in upper mantle attenuation, for which we had shown evidence in these papers, using here a more complete data set and a different, propagating wave approach. We also present maps of lateral variations in $1/Q$ as obtained from measurements of minor arc attenuation and their comparison with minor arc phase velocity maps. We attempt to take effects of focussing into account in a simple empirical manner based on the prediction from ray theory and compare the results with those obtained when ignoring these effects. We then discuss in more detail the depth extent of the degree 2 lateral variations in Q obtained and possible consequences for our understanding of the upper mantle models, in the framework of an absorption band model of anelasticity.

2. Data Set and Data Processing Method

We have selected 130 very long period vertical component records from the GEOSCOPE network, which are sampled continuously at 0.1 sample/s. For reasons which will become clear below, we have considered only records from large ($M_s > 6.7$), predominantly shallow events, for which the first four consecutive Rayleigh wave trains showed reasonable signal to noise ratio in the period range 100–400 s. The list of events used is given in Table 1. One advantage of using GEOSCOPE data, and the main reason why we relied only on data from this network, is that the large dynamic range of the instruments permits to record on scale, and without distortion, first arriving trains for events of magnitude greater than 7.5 at teleseismic distances. This was indeed verified, as we scanned the data set, except for a few records obtained at the beginning of the operation time of the network (1983–1984), when the dynamic range was limited by that of a temporary recording system. Most of our records were thus chosen in the later period of operation of the network, when data from at least five and in general more than 10 stations could be used for the same event.

For each record, each individual wave train was filtered by a variable filtering technique, which does not significantly distort the amplitude [*Cara*, 1973; *Roult and Romanowicz*, 1984], in order to extract the fundamental mode branch in as wide as possible a frequency range. This procedure is necessary to remove contributions from higher modes and separate the later arriving trains R3 and R4 from one another at the longest periods. Records for which R3 or R4 appeared too much contaminated by higher modes were not considered. This already resulted in a severe selection of data. An additional selection was imposed, after Fourier transforming the data to obtain phase and amplitude spectra, by discarding records corresponding to propagation in a direction far from that of maximum energy radiation and thus more sensitive to uncertainties in the source parameters and to off-path propagation effects. More specifically, we applied the following criterium: phase velocities were determined for the R1 and R2 trains, using two different sets of source parameters, and only those records were kept for which the phase velocities obtained using both solutions differed by less than 0.5% in the period range considered. As for the solutions, we used the centroid moment tensor (CMT) determination [*Dziewonski et al.*, 1981], on the one hand, and our own moment tensor solution on the other, obtained by inversion of very long period Rayleigh waves, using the method described by *Romanowicz and Guillemant* [1984] and *Romanowicz and Monfret* [1986]. In the few cases in which we did not have a reliable solution by the latter method, for the second solution we used the moment tensor solution from body waves (MT) as reported in the Preliminary Determination of Epicenters (PDE) bulletins [*Sipkin*, 1982]. The drawback of using the latter is that no estimate of the centroid time is given, which is an important parameter in phase velocity determinations, especially for the size of earthquakes considered. This selection serves two purposes: first, it leads to more accurate phase velocity determinations on minor arcs, which is a by-product of our study; as for the amplitudes, although we are able to eliminate point source effects by using four consecutive wave trains, as will be shown below, still we expect the effects of scattering and multipathing to be relatively stronger for near nodal paths, where the signal to noise ratio is poorer. Figure 1 shows the coverage of Earth obtained with the selected records. We note that it is much improved with respect to previous global attenuation studies of mantle waves.

Finally, we performed a last selection whose goal was to eliminate the frequency band, in each record, which would be clearly affected by either higher-order off-path effects or contamination by higher modes. This selection consisted in comparing great circle phase velocities obtained for waves travelling in opposite directions. For this we compared phase velocities measured between R1 and R3 on the one hand, R2 and R4 on the other, and discarded, for each record, the period ranges in which the difference was greater than 0.5%. In general, this affected only the longest periods ($T > 320$ s) and the shortest periods ($T < 120$ s), and very few data had to be eliminated at this point in the middle period range. Figure 2 shows an example of amplitude spectra for the R1 to R4 trains from one record. The portions of filtered wave trains from which the amplitude spectra originate are

TABLE 1. List of Events Used

Event	Date	Origin Time, UT	Latitude	Longitude	Depth, km	Magnitude M_s
Costa Rica	April 3, 1983	0205:1.1	8.72°N	83.12°W	37.	7.3
Hokkaido	June 21, 1983	0625:27.3	41.35°N	143.94°E	10.	6.9
Chagos	Nov. 30, 1983	1746:0.6	6.85°S	72.11°E	10.	7.6
Atlantic	Jan. 11, 1984	0448:50.2	8.19°N	38.79°W	10.	7.4
Kurile	March 24, 1984	0944:2.6	44.17°N	148.19°E	44.	7.0
Uzbek	March 19, 1984	2028:38.24	40.32°N	63.32°E	15.	7.0
Solomon	July 2, 1984	2133:21.49	10.02°S	160.47°E	18.	7.5
Sumatra	Nov. 17, 1984	0649:30.02	0.20°N	98.03°E	37.	7.2
Chile	March 3, 1985	2247:07.2	33.14°S	71.89°W	33.	7.8
Mexico	Sept. 21, 1985	0137:13.4	17.80°N	101.65°W	31.	7.6
Mexico	April 30, 1986	0707:18.1	18.40°N	102.97°W	27.	7.0
Aleutians	May 7, 1986	2247:10.8	51.52°N	174.78°W	33.	7.7
Molucca	Aug. 14, 1986	1939:13.6	1.80°N	126.52°E	33.	7.2
Romania	Aug. 30, 1986	2128:35.4	45.55°N	26.32°E	132.	6.9
Kermadec	Oct. 20, 1986	0646:9.9	28.12°S	176.37°W	22.	8.1
Taiwan	Nov. 14, 1986	2120:10.5	23.90°N	121.57°E	34.	7.8
Vanuatu	Jan. 3, 1987	2204:4.8	15.00°S	167.93°E	15.	6.5
Aleutians	Jan. 5, 1987	1211:55.7	52.45°N	169.38°W	30.	6.7
Atlantic	Jan. 30, 1987	2229:42.1	60.06°S	26.92°W	48.	7.0
Bismarck	Feb. 8, 1987	1833:58.3	6.09°S	147.69°E	33.	7.4
Chile	March 5, 1987	0917:05.2	24.39°S	70.16°W	62.	7.3
Ecuador	March 6, 1987	0410:41.9	0.15°N	77.82°W	10.	6.9
Vanuatu	Oct. 6, 1987	0419:06.0	17.94°S	172.23°W	15.	7.3
New Britain	Oct. 16, 1987	2048:01.6	6.27°S	149.06°E	48.	7.4
Alaska	Nov. 17, 1987	0846:53.3	58.59°N	143.27°W	10.	6.9
Alaska	Nov. 30, 1987	1923:19.1	58.68°N	142.79°W	10.	7.6
Chile	Jan. 19, 1988	0730:31.9	24.71°S	70.56°W	33.	6.7
Philippines	Feb. 24, 1988	0352:03.2	13.48°N	124.62°E	21.	7.0
Sandwich Isls	Feb. 26, 1988	0617:31.5	37.32°S	47.99°E	10.	6.7
Kamchatka	Feb. 29, 1988	0531:41.4	55.15°N	167.43°E	33.	6.8
Peru	April 12, 1988	2319:55.5	17.19°S	72.31°W	33.	7.0
Mexico	June 18, 1988	2249:42.3	26.86°N	110.99°W	10.	7.0
Aroe	July 25, 1988	0646:06.6	6.08°S	133.67°E	28.	6.7
Assam	Aug. 6, 1988	0036:24.6	25.14°N	95.12°E	10.	7.2
Solomon	Aug. 10, 1988	0438:26.1	10.37°S	160.82°E	34.	7.4
Tonga	Oct. 8, 1988	0446:24.5	18.77°S	172.42°W	35.	6.8
Armenia	Dec. 7, 1988	0741:24.2	40.99°N	44.19°E	10.	6.8
Molucca	Feb. 10, 1989	1115:24.6	2.31°N	126.76°E	44.	6.8
Kuriles	April, 11, 1989	0356:37.0	49.49°N	159.19°E	33.	6.6

also shown. For each source-station pair, the amplitude spectra for the four consecutive wave trains $R_1 \cdots R_4$ were then processed as described in section 3 to obtain estimates of minor arc and great circle attenuation as a function of frequency.

3. Separation of Focussing and Anelastic Effects

Separating effects of intrinsic attenuation from those of focussing due to lateral velocity variations is a difficult problem that has been ignored in the past and can only now start to be addressed owing to our progressively improving theoretical understanding. There can be two different approaches to this problem. The first is to try to correct for focussing effects directly, using higher-order amplitude calculations, either in the framework of ray theory [*Woodhouse and Wong*, 1986; *Romanowicz*, 1987] or in a more exact manner, using the variational method or higher-order perturbation theory [e.g., *Park*, 1987; *Tsuboi and Geller*, 1989; *Lognonné and Romanowicz*, 1990]. In particular, it was shown by *Davis* [1985] that a significant part of the variance in normal mode attenuation measurements could be attributed to scattering effects due to a large-scale lateral heterogeneity model. Such an approach implies that we are able to use an accurate enough 3-D velocity model. While this approach is being investigated further [e.g., *Romanowicz et al.*, 1989], we feel that it is not clear whether the velocity gradients in the presently available 3-D upper mantle models are well enough described to serve for the basis of realistic amplitude correction calculations. Indeed, while these models are able to explain observed waveforms rather well for well-behaved paths, a number of comparisons of observed and computed seismograms using available 3-D models [*Woodhouse and Dziewonski*, 1984; *Montagner and Tanimoto*, 1990] indicate poor agreement when observed amplitude anomalies are strong [e.g., *Lognonné*, 1989].

On the other hand, it is possible to try and correct for focussing effects without a priori assuming that the 3-D velocity model is well known, using an empirical approach based on the predictions of ray theory. The restriction is that it implies that the underlying structure is sufficiently smooth for ray theory to be valid, and therefore this can only be considered as a first step toward correctly accounting for focussing effects.

According to the results of ray theory [*Woodhouse and Wong*, 1986] or higher-order asymptotic theory [*Romanowicz*, 1987], the effects of focussing depend on the direction of travel along the great circle path containing epicenter and receiver. It is actually often observed that waves travelling

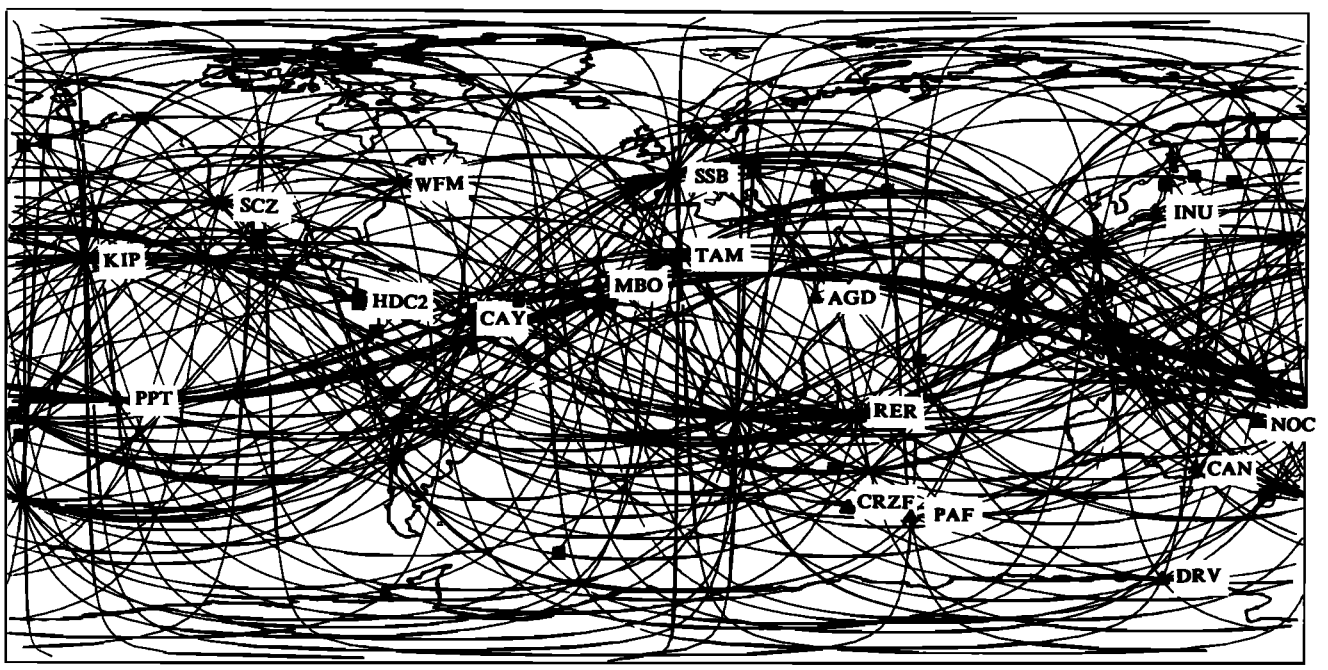

Fig. 1. Coverage of Earth obtained in this study. Epicenters are indicated by squares, stations by triangles.

in one direction (e.g., $R_1, R_3, \cdots$) are focussed, while waves travelling in the opposite direction are defocussed (e.g., R_2, $R_4, \cdots$), yielding the characteristic pattern of alternating high- and low-amplitude trains on the seismogram [e.g., *Lay and Kanamori*, 1985], a feature that cannot be produced by intrinsic attenuation. This is illustrated in the sketch of Figure 3. Focussing and defocussing effects depend on the relative position of the source (S), the receiver (R), their antipodes (S', R') and the heterogeneity which produces the focussing. Suppose, as shown in Figure 3, that there is a heterogeneous zone which produces focussing on the minor arc path between S and R. Then waves travelling in the minor arc direction (Figure 3*a*) will be focussed at R and its antipode R'; therefore all consecutive odd order trains will experience focussing at the receiver R. On the contrary, for even order trains (Figure 3*b*), R_2 will not be affected, but all consecutive trains will be focussed at S and S' and defocussed at R and R'. In reality (beyond ray theory), the situation can be, of course, more complex, since focal points are bound not to coincide with the source and the receiver, but the behavior in Figure 3 can be considered as a first-order description of the focussing effects.

More quantitatively, ray theory tells us that if we define δF_1, δF_g, and δF_2 to be the relative amplitude effects due to focussing along the minor arc (in the direction of propagation of R_1), along the great circle (in the direction of R_1) and along the major arc (in the direction of R_2) respectively, we should have the relations:

$$\begin{aligned} \delta F_g &= \delta F_3 - \delta F_1 \\ \delta F_g &= \delta F_1 - \delta F_2 \end{aligned} \tag{1}$$

The first relation stems from the definition of δF_g. The second one can be easily derived from the equations of *Woodhouse and Wong* [1986] or *Romanowicz* [1987]. Using the notations of *Romanowicz* [1987] and a mode summation approach, we have, in the process of converting from a mode approach to a propagating wave approach,

$$\begin{aligned} \delta F_1 &= -\frac{a}{U}\frac{\Delta \bar{D}}{2k} \\ \delta F_g = \delta F_3 - \delta F_1 &= -\frac{a}{U}\frac{2\pi \hat{D}}{2k} \\ \delta F_2 &= -\frac{a}{U}\frac{(\Delta \bar{D} - 2\pi \hat{D})}{2k} \end{aligned} \tag{2}$$

where a is Earth's radius, Δ is epicentral distance in degrees, U is group velocity, $k = l + \frac{1}{2}$, where l is the angular order of the mode, and

$$\bar{D} = \frac{1}{\Delta}\int_0^{\Delta} D(s)\, ds$$

$$\hat{D} = \frac{1}{2\pi}\int_0^{2\pi} D(s)\, ds$$

are minor arc and great circle averages, respectively, of a function D which depends on the first and second transverse derivatives of phase velocity along the great circle path.

On the other hand, intrinsic attenuation is additive along the path, regardless of the direction of travel, yielding the relations:

$$\begin{aligned} \eta_g X_g &= \eta_3 X_3 - \eta_1 X_1 \\ \eta_g X_g &= \eta_1 X_1 + \eta_2 X_2 \end{aligned} \tag{3}$$

where η_i is the attenuation coefficient along the path of train R_i, X_i is the distance travelled on this path, and the index g indicates a great circle average property. The change in sign

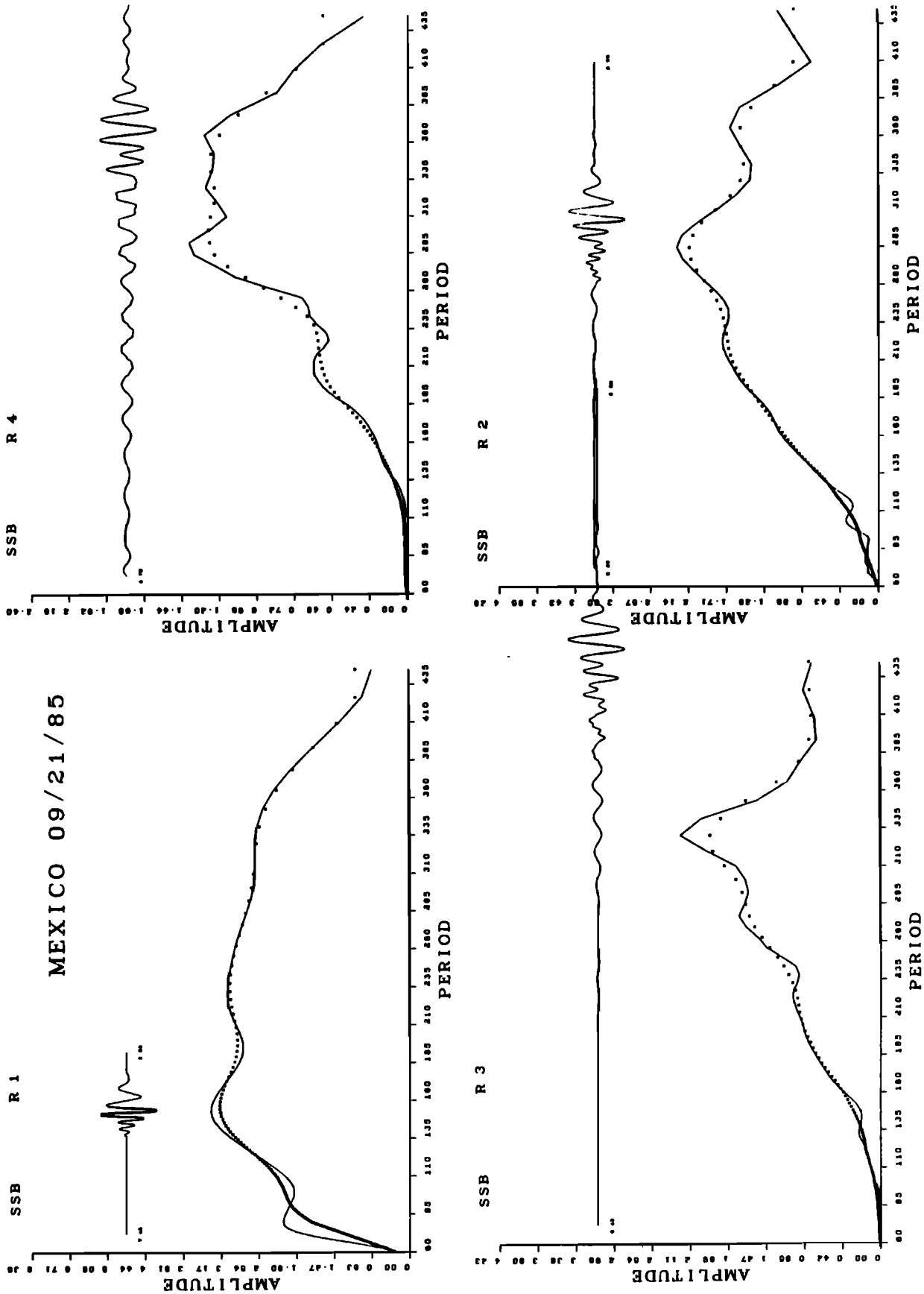

Fig. 2. Example of amplitude spectra for the first four Rayleigh wave trains of the Mexican aftershock of September 21, 1985, observed at station SSB. The portion of filtered record corresponding to each spectrum is shown.

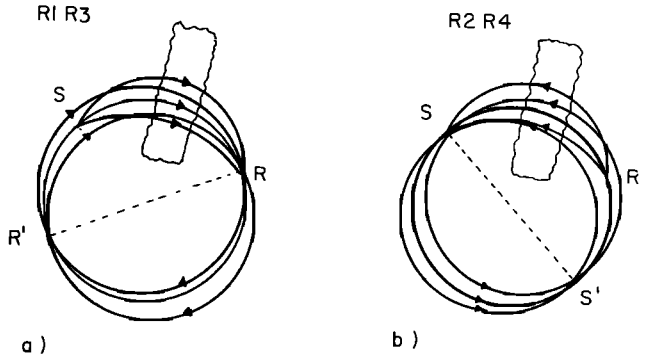

Fig. 3. Distinct focussing effects, as observed at station R, due to a heterogeneity located on the minor arc path (hatched area), for (*a*) waves circling in the minor arc direction, (*b*) waves circling in the major arc direction. S' and R' are antipodes of the epicenter S and station R, respectively.

between the second relations in equations (1) and (3) expresses the difference in effect due to focussing and intrinsic attenuation.

The determination of attenuation coefficients then proceeded as follows. The observed amplitude for a given wave train i at a given frequency ω can be written as the product of contributions from the source (A_s), the intrinsic attenuation, and the focussing terms:

$$A_i = A_s(1 + \delta F_i) \exp(-\eta_i X_i) \tag{4}$$

where $\eta_i(\omega)$ is the average attenuation coefficient along the path travelled, X_i is the distance travelled, and δF_i is the perturbation due to focussing, which we assume to be small. In equation (4), we have assumed a point source.

We then obtain the following set of equations for four consecutive trains:

$$\begin{aligned} \log A_1 &= \log A_s + \delta F_1 - \eta_1 X_1 \\ \log A_2 &= \log A_s + \delta F_1 - \delta F_g + \eta_1 X_1 - \eta_g X_g \\ \log A_3 &= \log A_s + \delta F_1 + \delta F_g - \eta_1 X_1 - \eta_g X_g \\ \log A_4 &= \log A_s + \delta F_1 - 2\delta F_g + \eta_1 X_1 - 2\eta_g X_g \end{aligned} \tag{5}$$

We recall that for focussing terms, the great circle properties (δF_g) are here oriented in the direction of propagation of the minor arc.

We see that $\log A_s$ and δF_1 are always combined and cannot be separated, but the linear system of four equations in the four unknowns η_1, η_g, δF_g, and ($\log A_s + \delta F_1$) has a nonzero determinant; therefore it can be solved for each seismogram to obtain estimates of attenuation along the minor arc, attenuation on the great circle path, as well as the average great circle focussing effect.

If we set focussing effects to zero, equations (5) become an overdetermined system which can be solved for attenuation terms alone. In what follows, we will compare results obtained under the assumption of "no focussing" and under the assumption that focussing can be described as in equations (5). We note here that the use of at least three consecutive trains allows us to eliminate the error on the source amplitude (at least under the assumption of a point source). This is an important point, since this type of error can be very large and since we discard near-nodal paths rather drastically, mainly due to the large uncertainty in the estimation of the scalar moment, which can often be of the order of 50–100%. In consequence, while the uncertainty in the source phase is small enough to allow the determination of stable global phase velocity maps using first arriving trains [e.g., *Nataf et al.*, 1986], this is not possible at present with amplitude data. An experiment performed using our data set, with measurements of amplitudes on R_1 and R_2 trains only, and source parameters as given by CMT solutions [*Dziewonski et al.*, 1989] has convinced us early on to abandon such an approach.

We have thus proceeded in two steps. First, we have obtained a collection of minor arc and great circle average attenuation coefficients in the period range 350–90 s by applying equations (5) for each record. Then we have inverted this data set to obtain maps of lateral variations of the local quality factor for Rayleigh waves. The results of this two-step inversion will be presented in the next sections. The attenuation coefficients will be converted into temporal Q by using the classical relation [*Aki and Richards*, 1980]:

$$\text{temporal } Q = C/U \text{ spatial } Q$$

where U is group velocity.

4. Global Maps of Rayleigh Wave Attenuation

We here present geographical maps of lateral variations in $1/Q$, obtained from the measurements of attenuation coefficients on a collection of globally distributed paths, as described in section 3. These maps have been obtained by regionalizing the path averages using a modification of the method without a priori constraints designed by *Montagner* [1986] for a study of the Indian Ocean and adapted to the global case. This method introduces covariance functions in the data and model space and a correlation length which determines the smoothness of the model. It has the advantage over a classical spherical harmonics decomposition in that it does not introduce spurious extrema at regular spacing when the spherical harmonics series is truncated at low degree. A correlation length of 5000 km was chosen, in view of the trade-off between the details of the model and a posteriori errors. The Q maps corresponding to each period, expressed in terms of relative variations in $1/Q$ with respect to the average value at that period, are presented together with similarly obtained local frequency maps. In the latter, phase velocity regionalized from great circle data (using the phase difference between R_1 and R_3), or minor and major arc data were converted to local frequencies. The use of the first arriving trains provides better resolution of the odd terms of lateral heterogeneity, as shown, for example, by *Monfret and Romanowicz* [1988]. We will first show the maps obtained from great circle average and minor arc measurements, and in section 5 we will discuss the degree 2 pattern observed in more detail.

4.1. *Great Circle Averages*

Plate 1 is a comparison of local frequency and ($1/Q$) maps at a period of 200.85 s (angular order $l = 43$) derived from great circle averages. (Plate 1 is shown here in black and white. The color version can be found in the separate color section in this issue.) The dominant degree 2 pattern in the local frequency map is consistent with previous studies of this kind. The $1/Q$ map is characterized by high attenuation

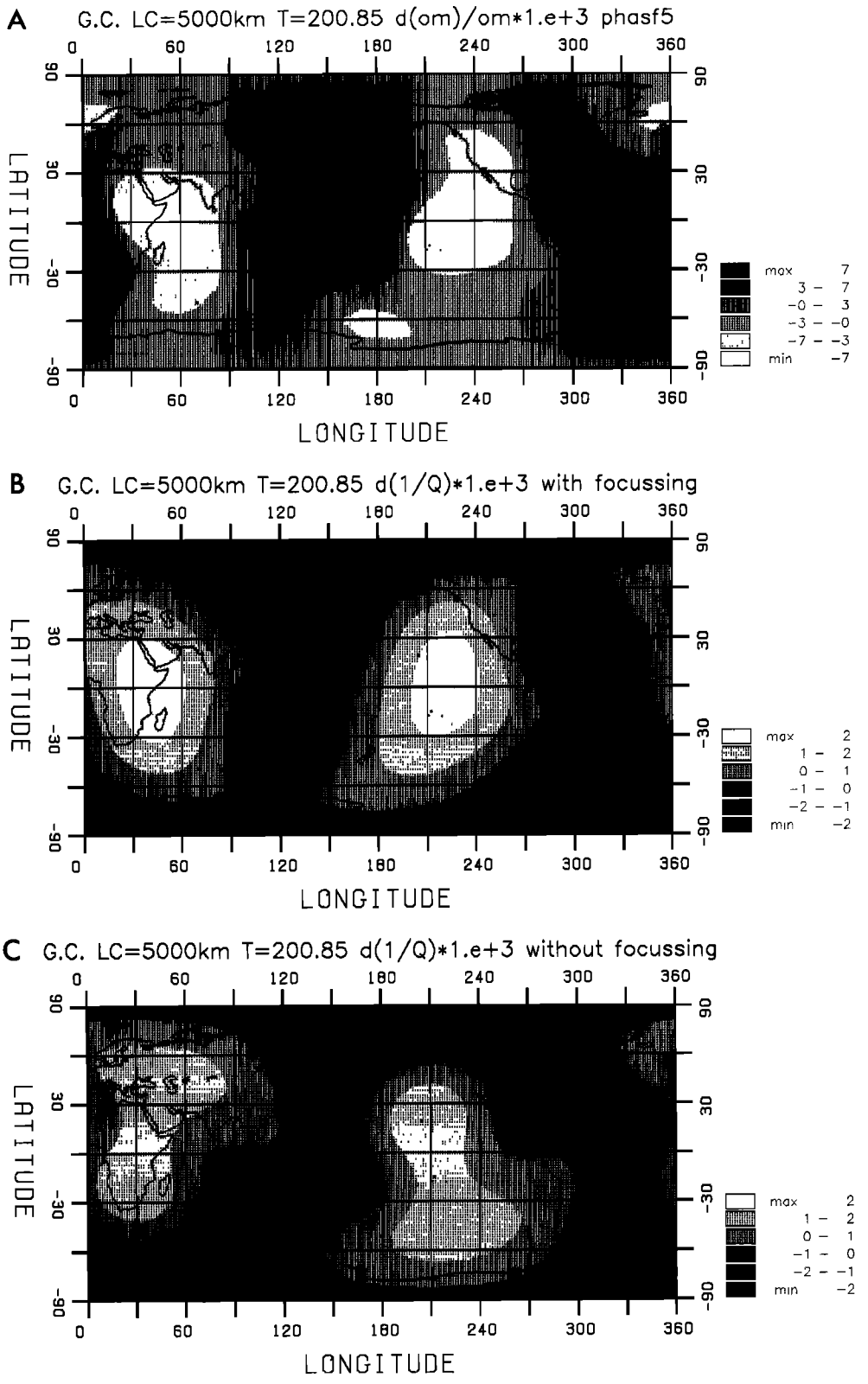

Plate 1. Maps obtained at a period of 200.85 s from great circle data, using a correlation length of 5000 km. (The color version and a complete description of this figure can be found in the separate color section in this issue.)

in the central Pacific and Indian Ocean and low attenuation over the western Pacific subduction zone and the Atlantic Ocean. Lateral variations in Q reach 35–40% compared to 1% in the local frequency map. A posteriori standard errors in the $(1/Q)$ maps are rather uniformly distributed and of the order of 1.2×10^{-3}, for an assumed 15% error in the data. These errors are, as expected, rather large, but the larger-scale features are well resolved. The clear degree 2 pattern in

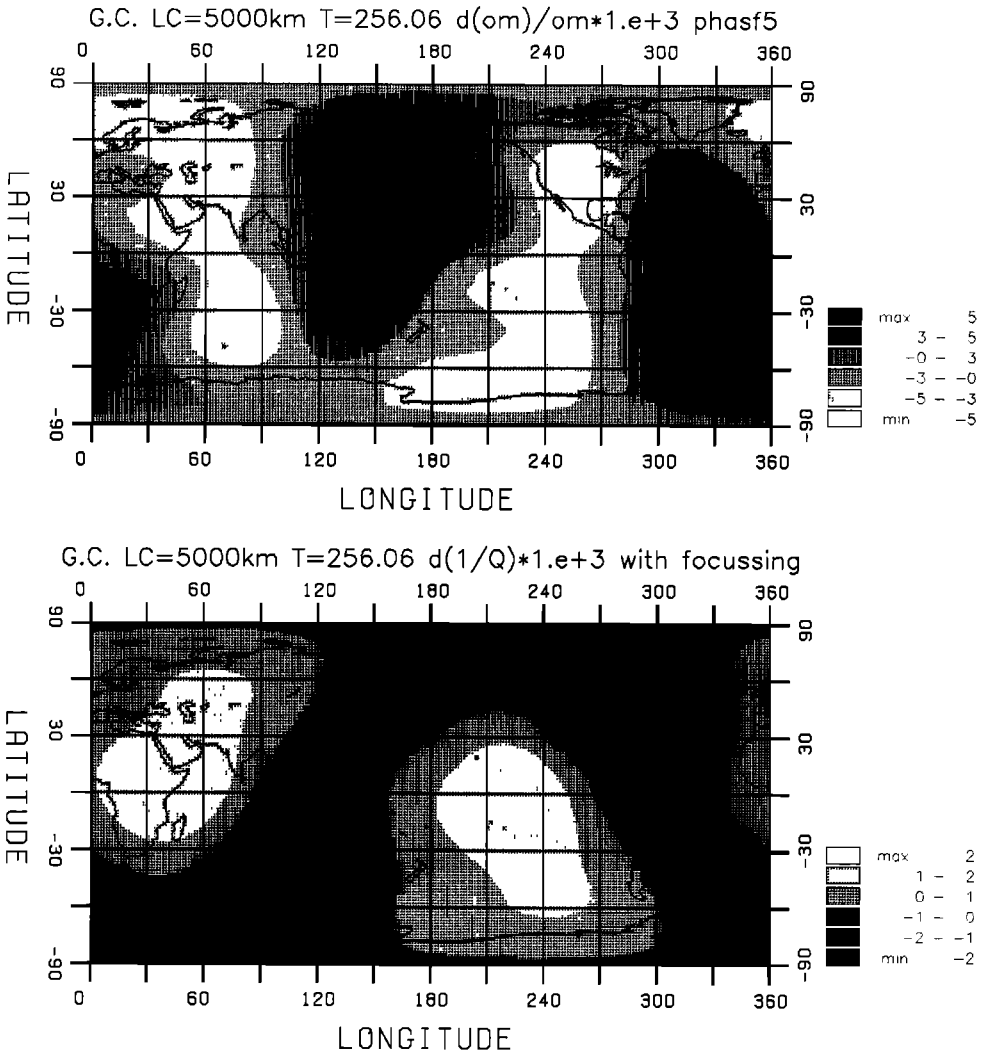

Fig. 4. Maps of relative variations in local frequency (top) and variations in $1/Q$, after taking focussing effects into account (bottom) at a period of 256.06 s. See caption of Plate 1 for units. Extremal values are +0.9% and −0.7% for local frequencies, and $+1.9 \times 10^{-3}$, -1.6×10^{-3} for $\delta(1/Q)$.

the attenuation map is just as striking as in the local frequency map and confirms our earlier observations based on spheroidal mode attenuation measurements [*Romanowicz et al.*, 1987; *Roult et al.*, 1990]. We note the correlation of high attenuation with low phase velocity and a slight shift toward the west of the Q extrema with respect to the phase velocity extrema. While most striking at periods around 180–200 s, this correlation persits to some extent at longer periods (Figure 4; T = 256 s) and shorter periods but disappears at 300 s (Figure 5) and 125 s (Figure 6). Plate 1*c* shows the ($\delta(1/Q)$ map obtained at 200.85 s by measuring amplitude ratios between R3 and R1, without any correction for focussing and the same data set as used in Plate 1*b*. The pattern in Plate 1*c* is similar to that of Plate 1*b*, but the maximum amplitudes are smaller by a factor of 1.5, so that the degree 2 pattern barely comes out of the noise. We interpret the weakness of the pattern in Plate 4*c* as being related to the degree of incoherency of the dataset not corrected for focussing effects. This is supported by the greater variance reduction achieved at low degrees with the dataset corrected for focussing (e.g., Figure 12). The correction for focussing has an effect of "cleaning" the data set similar to that of keeping only the best behaved paths but allows to work with a larger data set and thus to obtain better spatial resolution. In fact, we find that the derived focussing terms often have the same order of magnitude as the attenuation terms. This problem will be addressed further in section 5, in which we will analyze the degree 2 effect in the Q maps more quantitatively, making use of a spherical harmonics expansion of the attenuation data. One may also wonder whether the uneven sampling of the sphere as visible on Figure 1 (although somewhat exaggerated by the Mercator projection) does not bias the resulting degree 2 seen in Plate 1. In fact, when performing the spherical harmonics expansion to study the degree 2 in more detail in section 5, we have used averages over 5° by 5° bins of great circle poles in order to minimize this potential bias.

In order to quantify the observed correlation between local frequency and Q, we have calculated the correlation coefficient, as a function of period, between the great circle average attenuation and the great circle average local frequency, for the data sets used in Plates 1*a* and 1*b*, taken path

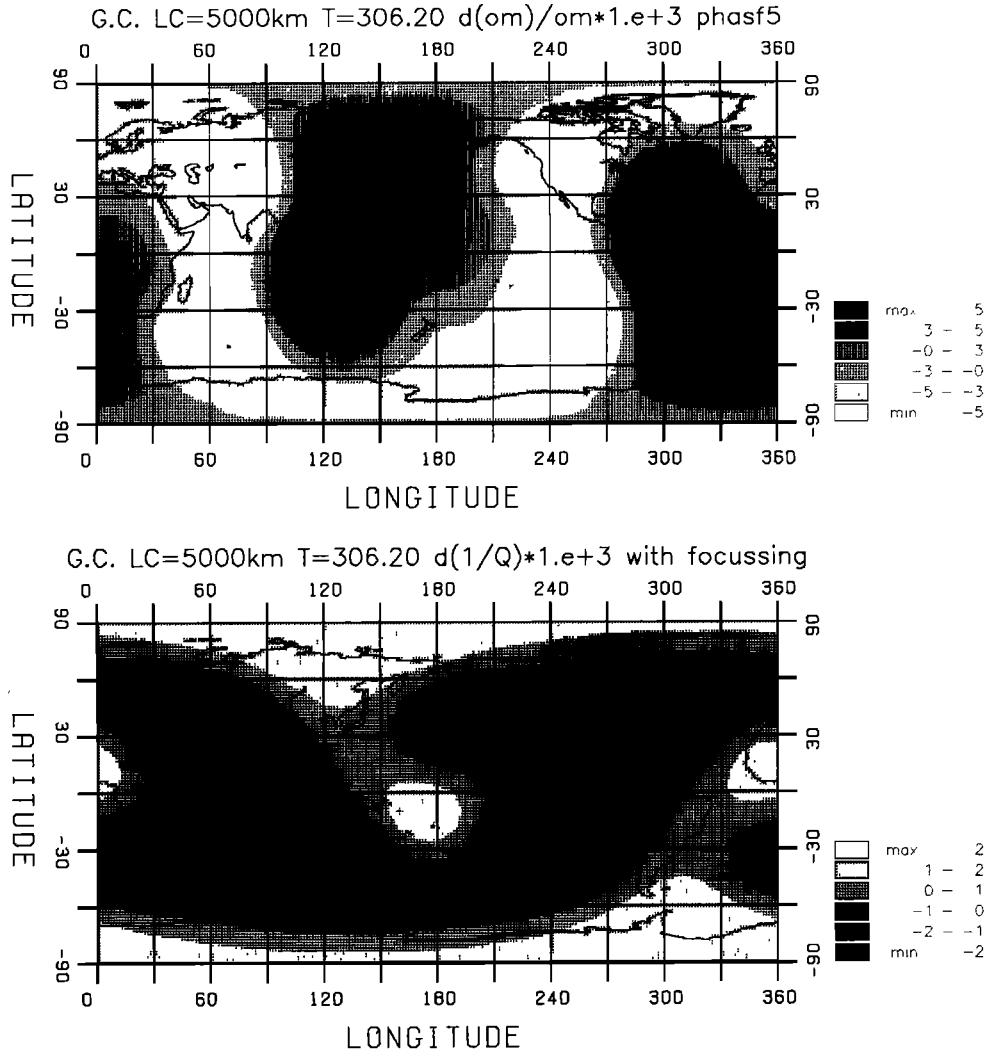

Fig. 5. Same as Figure 4 at a period of 306.20 s. Extremal values are +1.5% and −0.9% for local frequencies, $+2.1 \times 10^{-3}$, -2.5×10^{-3} for $\delta(1/Q)$.

by path. This is shown in Figure 7, along with the correlation coefficient obtained when focussing is not taken into account (Plates 1*a* and 1*c*). As expected, this correlation coefficient is maximum around 180–200 s and larger for the data set where focussing has been taken into account. Another way of estimating the correlation is by comparing maps in Plates 1*a* and 1*b*, taking values at 10° by 10° grid points one by one. Table 2 gives a list of the correlation coefficients obtained by shifting one map with respect to the other by steps of 10° in longitude. The correlation is good for a zero shift but best when the local frequency map is shifted by 30° to the east compared to the attenuation map. This is in good agreement with the observations. We shall see in section 5 that we do not expect the correlation between these observations to be much higher, if it originates in a layer localized in depth.

4.2. *Minor Arc Averages*

In Plate 2*a* and Figure 8 we present examples of maps of lateral variations in attenuation with odd degrees included (minor and major arc data), after correcting for focussing effects using equations (5). (Plate 2 is shown here in black and white. The color version can be found in the separate color section in this issue.) Plate 2*a* also shows the map of lateral variations in local frequency obtained at 200.85 s. As in the case of the great circle data, a striking correlation appears between the large-scale features of both types of maps, especially at periods of around 200 s, with lowest velocities and highest attenuation in the east central Pacific and the Indian Ocean and higher velocities and lower attenuation in the Atlantic and the western Pacific. To assess the degree of confidence in our attenuation maps, we will discuss the map at 200 s more carefully here. The local frequency map indicates lateral variations of the order of 1–1.5%, in agreement with results found in previous studies, and the geographical distribution in the map is, in general, also consistent with models presented in those studies. The attenuation map shows, as expected, much larger variations, of the order of $\pm 6 \times 10^{-3}$ in $(1/Q)$, with peaks to ± 8–10^{-3}, or over 100% in Q. For comparison, Plate 2*c* shows the attenuation map obtained at 200.85 s without taking into account focussing effects, but using only R1, R2, and R3 trains to eliminate the uncertainty on the source amplitude.

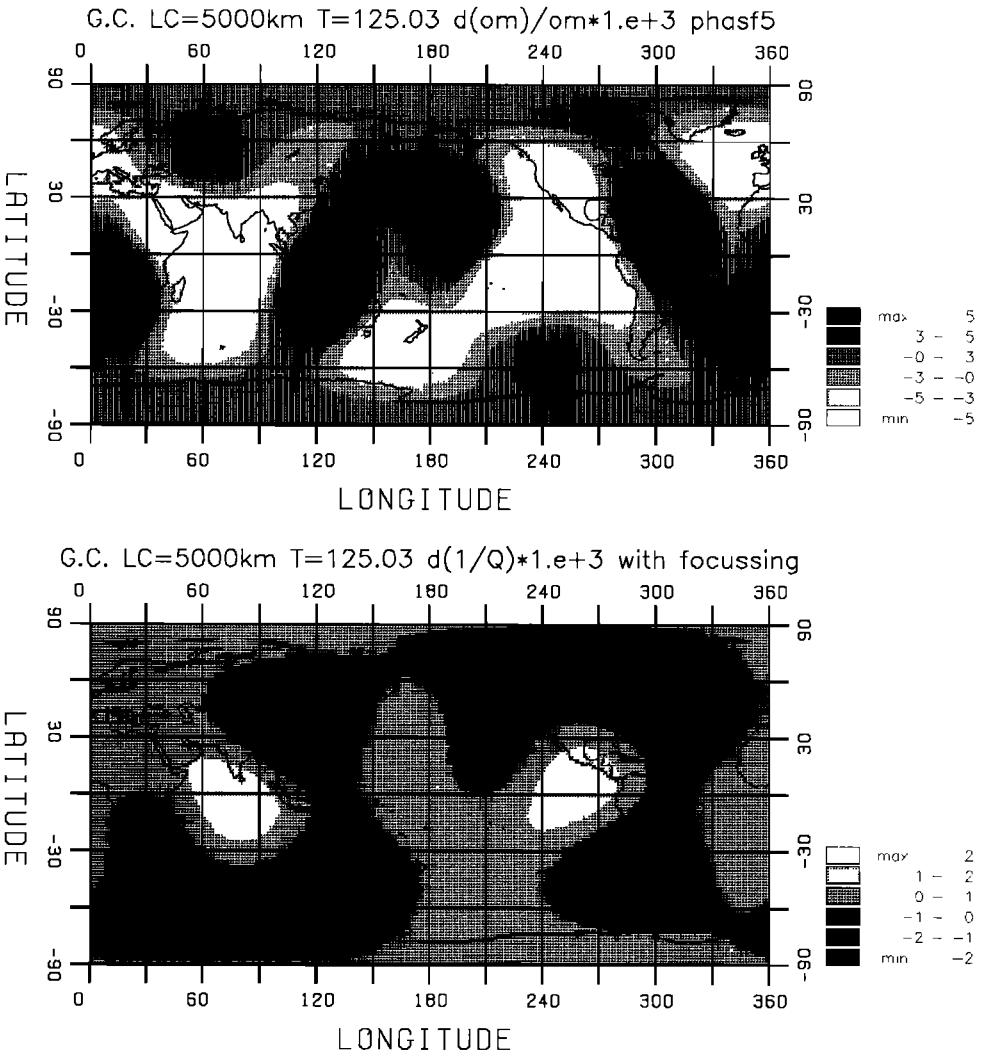

Fig. 6. Same as Figure 4 at a period of 125.03 s. Extremal values are +1.3% and −1.3% for local frequency, $+1.8 \times 10^{-3}$ and -1.5×10^{-3} for $\delta(1/Q)$.

The order of magnitude of lateral variations in $(1/Q)$ is the same, and the maps in Plates 2*b* and 2*c* display many of the same features, the major differences arising in the Indian Ocean and Red Sea region. It is important to assess whether the large lateral variations are real or exaggerated, and we should keep in mind that in this type of inverse problem, the resulting pattern of anomalies is usually much more stable than their absolute amplitudes, which can be affected by outside factors such as the nonuniform distribution of paths, and a priori assumptions on the allowed variance in the model [*Tarantola and Valette*, 1982]. Here we have assumed an a priori variance in the model of 50%, based conservatively on expected lateral variations in $1/Q$ from previous studies, with errors in the data estimated to be of the order of 15%. It is also important to decide whether correcting for focussing effects in the manner proposed here improves the accuracy of the maps obtained. Here, we have performed the following "direct" experiment.

In regions where the two maps differ significantly, we have tried to find examples of data where we could calculate attenuation on relatively "pure" paths between two stations aligned with an epicenter. Although such examples are hard to come by, this has been possible in the Indian and Pacific oceans. The first example is for the Romanian earthquake of August 30, 1986, observed at stations AGD and RER, aligned to within 1° of a great circle with the epicenter. Figure 9*a* shows the amplitude spectra for this event at these two stations, after correcting for instrument response and geometrical spreading. While the raw spectra look perturbed below 120 s, probably due to interference with higher modes for this intermediate depth (140 km) event, this is not a problem at longer periods. The inferred value for $\delta(1/Q)$ between the two stations is $\simeq 5\ 10^{-3}$ at 200 s, corresponding to a Q value of about 83, and in better agreement with Plate 2*b* obtained after correcting for focussing than with Plate 2*c* without the correction. We note that these data have not been used in the inversion leading to Plate 2*b* because of too noisy R_4 trains. We have not been able to find any other case of two stations aligned with an epicenter in this region, but we have also analyzed the amplitude spectrum observed for R1 at station PAF for the Chagos event of November 30, 1983, for a path entirely contained in the highly attenuating region of Plate 2*b*, using the source parameters provided by the CMT solution [*Dziewonski et al.*, 1982]. In this case, we

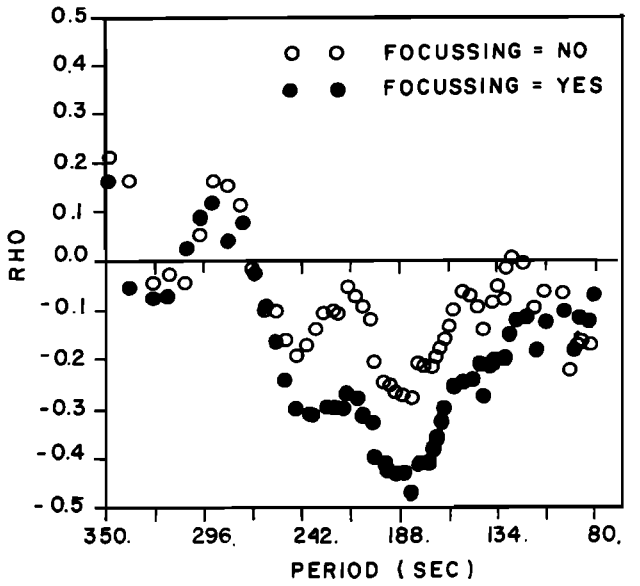

Fig. 7. Correlation coefficient as a function of period, calculated path by path, between phase velocity and attenuation coefficient on great circle paths, with and without taking focussing effects into account. High attenuation coefficient corresponds to low velocities, giving the negative sign for ρ around 200 s, where the correlation is strongest.

obtained very similar results, also with an estimate of $\delta(1/Q)$ of 5×10^{-3}. On the other hand, the map obtained without correction for focussing would predict considerably higher Q values. In the Pacific, we have measured the amplitude ratio at 200 s for an event in Mexico (April 25, 1989) observed at stations PPT and CAN. These data for a very recent event also have not been used in the inversion. The amplitudes of R1 at both stations are shown in Figure 9*b*. The path between these stations (also aligned to within 1° of a great circle with the epicenter) falls on the boundary between lower and higher than average $\delta(1/Q)$ in the map of Plate 2*b*, while Plate 2*c* would predict much higher Q. We have measured $\delta(1/Q) \simeq 0.5 \times 10^{-3}$ for this path, corresponding to a Q of 140, quite close to PREM and in good agreement with Plate 2*b*. The examples shown here indicate that at least in the regions sampled, correction for focussing as we have done may be useful. Of course, these comparisons are only qualitative and are intended to verify orders of magnitude rather than precise values of local attenuation, given the large correlation length imposed on our maps. However, we do present some evidence for departures from PREM, at 200 s, of the order of 75%, indicating that the lateral variations in $(1/Q)$ given in Plate 2*b* have the correct order of magnitude but that the extrema in this map are probably somewhat exaggerated.

TABLE 2. Correlation Coefficient ρ between Plates 1*a* and 1*b* as a Function of Shift by K Increments by 10° to the East, of Plate 1*b* With Respect to Plate 1*a*

K	ρ
0	−0.523208
1	−0.628572
2	−0.652495
3	−0.590213
4	−0.453295
5	−0.265161
6	−4.777040E-02
7	0.179737
8	0.391537
9	0.547694
10	0.617653
11	0.600808
12	0.516841
13	0.382706
14	0.203987
15	−1.991879E-02
16	−0.266730
17	−0.487997

E − 02 = $\times 10^{-2}$.

We have not been able, as yet, to find any pure paths in a region of high Q in Plate 2 to assess the validity of the amplitudes in such regions. We can nevertheless discuss our results in the light of previous studies. In his global Q study by regionalization according to tectonic province, *Nakanishi* [1979*a*] found large variations in excess of 50% at 200 s. Assuming that the variation with frequency of intrinsic Q is not significant between 30 and 200 s, we can also compare our results to those obtained previously from the study of multiple *ScS*. For example, *Sipkin and Jordan* [1980] measured high Q_{ScS} at long periods, along subduction zones in Japan and South America, and low Q_{ScS} on different paths across the Pacific ocean, implying lateral variations of more than 50% in upper mantle Q if one assumes little lateral variation in Q in the lower mantle. Moreover, they inferred a correlation between the variations in $(1/Q)$ and the corresponding *ScS* relative travel anomalies of the form $\delta(1/Q) = 0.4\delta T/T$, where T is the travel time of *ScS*, which is consistent with our results, if we exclude the extremal values in our maps. We note, however, that these authors inferred a higher Q in South America than in the Kurile-Japan portion of the western Pacific suduction zone, contrary to our results. This discrepancy should be investigated further, as more data become available leading to a better spatial resolution in our maps.

The maps shown here represent a first attempt at obtaining a global image of lateral variations of Q at mantle wave periods without any a priori assumptions on their relation to either tectonic features or corresponding phase velocity maps. While this image is still very coarse and the details will probably change as more data become available, we have presented evidence in support of some correspondence between the lateral variations of Q and the velocity distribution at periods around 200 s, with low Q values in the eastern and central Pacific as well as the Indian ocean and high Q values over most of the Atlantic as well as Eurasia and the northern hemisphere part of the western Pacific subduction zones. The correlation with the phase velocity map in Plate 2 is qualitative and can be assessed visually. A shift to the west of the largest-scale features in the attenuation map is apparent in Plate 2, just as was the case in Plate 1. We will, however, not attempt to discuss these results any more quantitatively except for the degree 2 pattern, for which our results are the most robust, given the spatial coverage of our data.

5. The Degree 2 Pattern in Attenuation: Analysis and Discussion

Since the most striking feature in Plate 1 and Figures 4 and 5 is a degree 2 pattern apparent in the $1/Q$ maps, in good

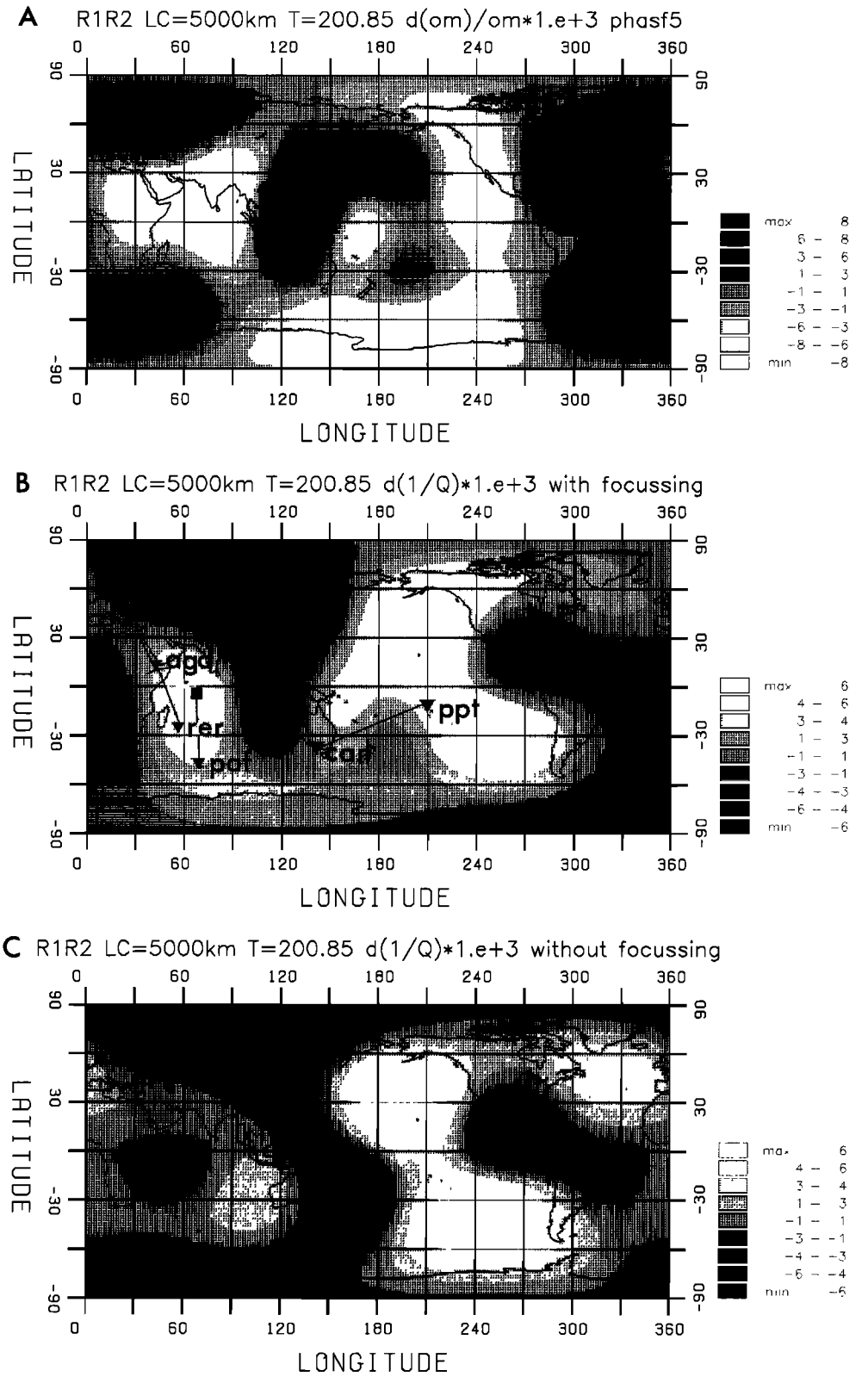

Plate 2. Local frequency and attenuation maps obtained at a period of 200.85 s from minor and major arc data, using a correlation length of 5000 km. (The color version and a complete description of this figure can be found in the separate color section in this issue.)

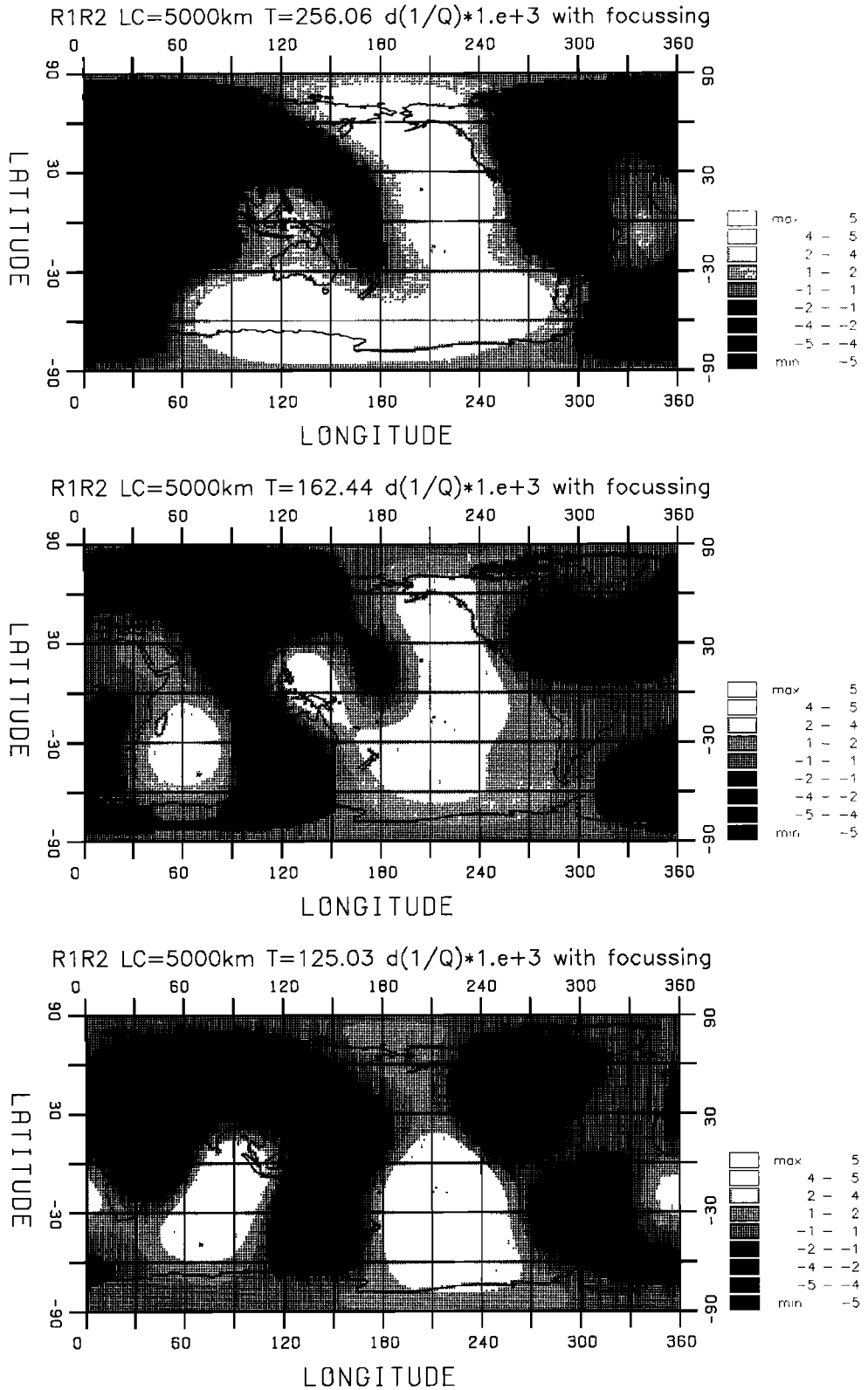

Fig. 8. Maps of lateral variations in $(1/Q)$ obtained using minor and major arc data, at different periods, after correcting for focussing using equations (5). Units are as in Plate 2. (*a*) 256.06 s, extremal values are $+6.5 \times 10^{-3}$ and -5.3×10^{-3}; (*b*) 162.44 s, extremal values are $+5.5 \times 10^{-3}$ and -5.5×10^{-3}; (*c*) 125.04 s, extremal values are $+10.2 \times 10^{-3}$ and -7.2×10^{-3}.

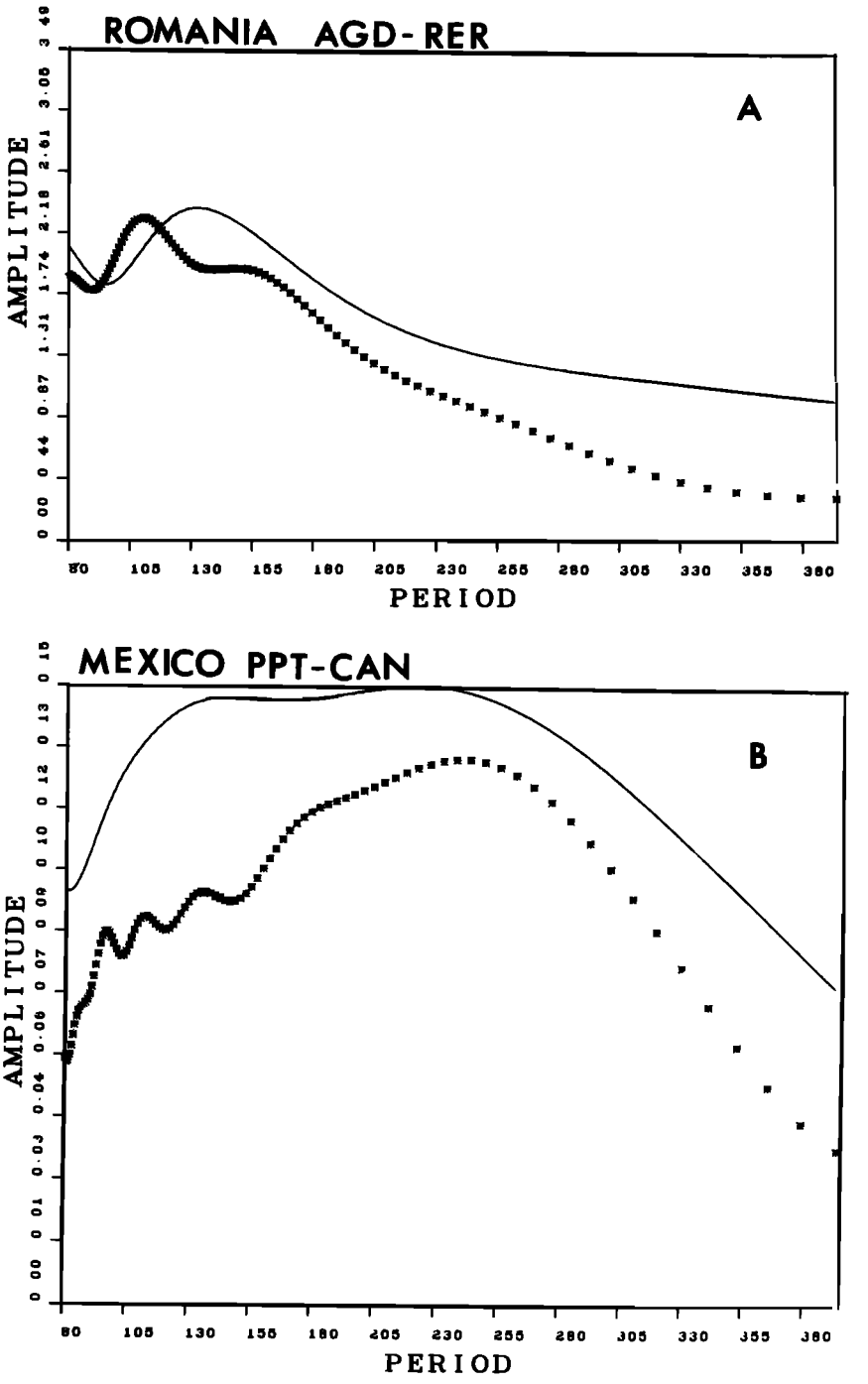

Fig. 9. Amplitude spectra for R1 used in the two station measurements described in the text. The spectra have been corrected for instrument response and geometrical spreading. (*a*) Romanian event of August 30, 1986, observed at stations AGD (solid line; Δ = 36.8°; azimuth = 152.22°) and RER (dotted line; Δ = 71.72°; azimuth = 151.04°). (*b*) Mexican event of April 25, 1989, observed at stations PPT (solid line; Δ = 60.14°; azimuth = 237.77°) and CAN (dotted line; Δ = 117.05°; azimuth = 238.72°).

correspondence with the well-documented degree 2 seen in velocity maps, it is worthwhile to examine this point in more detail. We have thus performed a spherical harmonics expansion of the great circle average Q data up to degree 2 and 4 and analyzed the variation with period of the degree 2 coefficients. As mentioned earlier, before expanding into spherical harmonics, we have taken averages corresponding to great circles whose poles fell inside 5° by 5° "squares," thus improving the uniformity of the distribution of data. The spherical harmonics expansion is performed according to the definition

$$f(\theta, \phi) = \sum_{l} \sum_{m=0}^{m=2l+1} X_l^m(\theta)(C_{lm} \cos m\phi + S_{lm} \sin m\phi)$$

where X_l^m are related to the Legendre functions by

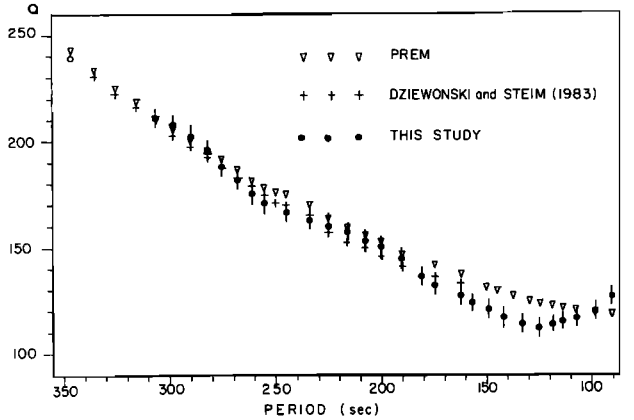

Fig. 10. Globally averaged Q of fundamental spheroidal modes obtained here as compared to model PREM and the measurements of *Dziewonski and Steim* [1982].

$$X_l^m(\theta) = (-1)^m[(2l+1)(2-\delta_{0m})]^{1/2}\left[\frac{(l-m)!}{(l+m)!}\right]^{1/2} P_l^m(\theta)$$

A first by-product of this analysis is the determination of a globally averaged Rayleigh wave Q as a function of period. The resulting values are compared to previous models in Figure 10. The stability of this determination has been checked by comparing the values obtained from spherical harmonics expansions up to degree 2 and 4. Our measurements agree both with the PREM model and the model obtained by *Dziewonski and Steim* [1982] between periods of 300 and 120 s. We obtain somewhat lower Q values below that period, and we note a minimum at $T = 130$ s as compared to $T = 90$ s in the PREM model [*Dziewonski and Anderson*, 1981]. On the other hand, our average Q values between periods of 300 and 200 s are systematically lower by about 10% than those obtained by *Smith and Masters* [1989] using normal modes and an entirely different approach. The reason for this discrepancy needs to be investigated further.

Figure 11 shows the power in degree 2 as a function of decreasing period for $1/Q$. In agreement with the visual results of Plate 1 and Figures 4–7, we observe a peak in the degree 2 power at periods of 180–200 s, coincident with the peak observed earlier in the frequency shift measurements [*Romanowicz et al.*, 1987]. The degree 2 pattern in attenuation corresponds to lateral variations in Q of about 25% at its peak. Figure 12 shows the variance reduction for the degree 2 expansion. In Figure 12, we compare the variance reduction obtained on the one hand, with the data set of attenuation coefficients obtained when taking into account the focussing terms according to equation (2), and on the other hand, with the data set consisting of R3 to R1 amplitude ratios, ignoring other effects beside intrinsic attenuation. In the former case, the variance reduction reaches 35% at a period of about 200 s and is stronger than when focussing terms are ignored. This strong variance reduction peaking around 200 s confirms the results inferred previously from

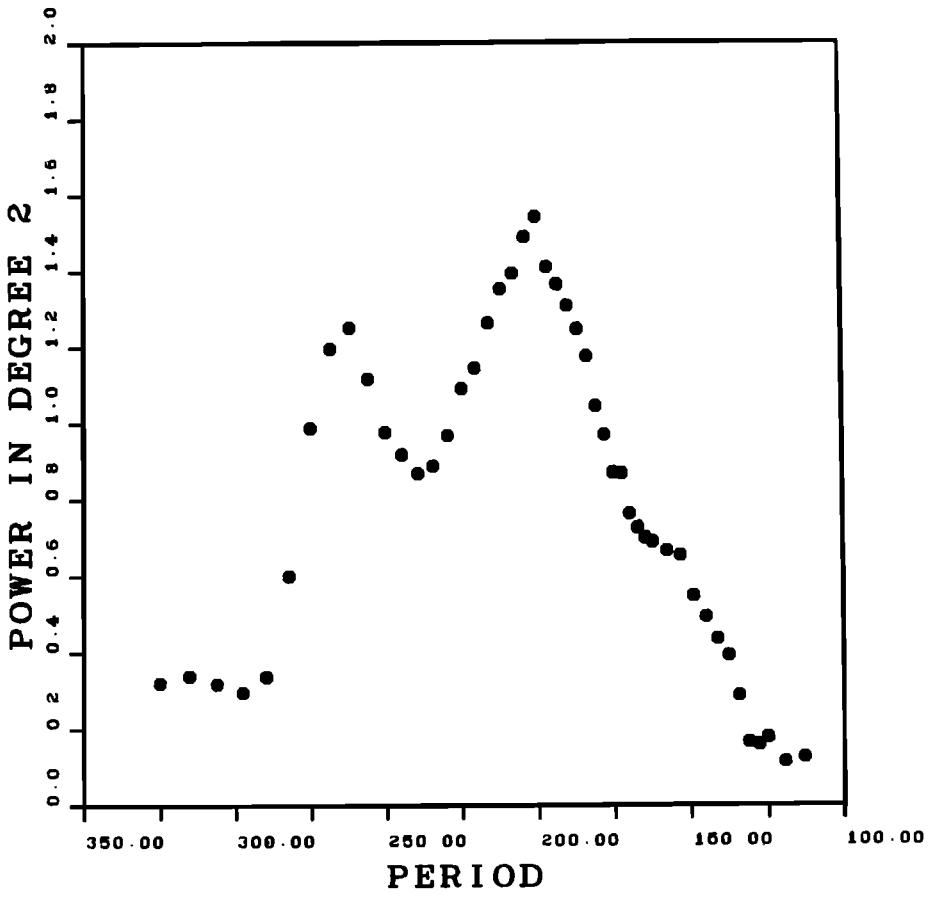

Fig. 11. Power in degree two as a function of period for $1/Q$, when focussing is taken into account.

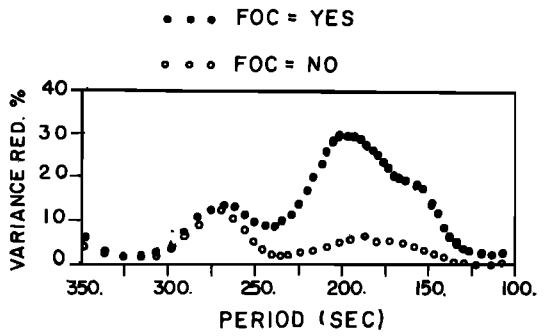

Fig. 12. Variance reduction in Q as a function of period for the degree 2 expansion, for the data set consisting of R3/R1 amplitude ratios (open circles) and for the data set consisting of great circle average attenuation coefficients after focussing effects have been taken into account.

normal mode attenuation measurements [*Romanowicz et al.*, 1987] and points to the significance of the degree 2 pattern, in spite of larger errors in the measurements than for eigenfrequencies or phase velocities. The variance reduction in the second case is much less significant. This corroborates the results of section 4: allowing for focussing effects produces a global data set of great circle attenuation measurements that contains much less scatter and is better behaved in its lowest-wavelength features and that we have indeed succeeded, to some extent, in "cleaning" the data of unwanted effects.

Figure 13 presents the 5 individual degree 2 coefficients in $1/Q$, and in order to show the stability of the results, we compare the plots obtained for a spherical harmonics expansion up to degree 2 (Figure 13*a*) and up to degree 4 (Figure 13*b*). We note that the best resolved component, which gives its shape to the power in degree 2 distribution in Figure 12, is the S_{22} component. This is in agreement with our previous free oscillation results and is also strikingly reminiscent of the results of the degree 2 expansion of fundamental spheroidal mode frequency shifts, for which the variation with frequency of the degree 2 coefficients is given in Figure 14 for reference. We note that S_{22} has a peak at about the same period both in the case of $1/Q$ and in the case of $\delta\omega/\omega$. On the other hand, the C_{22} component is much weaker and poorly resolved in the attenuation data. Since the relative amplitude of the C_{22} and S_{22} terms determines the position of peaks and zeroes in longitude of the degree 2 pattern in the maps of Plate 1 and Figures 4 and 5, the difference in this ratio for frequency shifts and attenuation explains the shift toward the west observed in the patterns of attenuation coefficient in Plate 1. In addition, the difference in behavior of the C_{22} term in $1/Q$ and in $\delta\omega/\omega$ indicates that the correlation in the S_{22} terms cannot be an artifact of the measurement procedure: if the measurement of amplitudes was strongly affected by lateral variations in the velocity structure, causing apparent, but strongly biased correlation between attenuation and phase velocity maps, one would expect the correlation to appear in all resolved degree 2 components, which is not the case. The other stronger degree 2 component in Q appears to be C_{20}, at least at periods below 200 s, but we will not attempt to interpret this component at this point, since ellipticity corrections in attenuation have not been accurately taken into account: only the external ellipticity of figure of Earth, entering through the length of the great circle, has been corrected for, whereas for local frequencies, a complete ellipticity correction calculated using Clairaut's theory for hydrostatic equilibrium [*Dziewonski and Sailor*, 1976] was applied.

Plate 1 and Figures 4, 5 and 11–13 clearly indicate the existence of a strong degree two pattern in Q, which peaks around 200 s, implying that the corresponding lateral variations in intrinsic attenuation of the mantle are concentrated in depth, of course, if one assumes that there is no significant frequency dependence of Q within the range of our study. Without performing a formal inversion, which we postpone until a more dense data set can be assembled, we can infer that this region of the upper mantle corresponds to a depth range of 250–500 km, in agreement with the depth range proposed in our frequency shift study, in which we inverted for the best fitting one-layer heterogeneity [*Romanowicz et al.*, 1987] and later for heterogeneity distributed in the upper mantle [*Roult et al.*, 1990].

The results presented here confirm the inferences made in our previous study of free oscillation frequencies and attenuation. The degree 2 distribution in the upper mantle is concentrated in two regions: a shallow layer on the one hand, corresponding to the distribution of tectonic provinces and expressed in the C_{22} term of the degree 2 spherical harmonics expansion of local frequency but not in that of Q, and, on the other hand, a deeper layer, located in the depth range 250–500 km and expressed in the S_{22} component of both local frequency and attenuation (it is thus offset by about 45° to the west with respect to the shallow degree 2 pattern). This deeper, most prominent layer, is, however, somewhat shallower than inferred in previous modeling [*Masters et al.*, 1982; *Woodhouse and Dziewonski*, 1984] due probably to the fact that these studies had, respectively, less resolution at high frequency and a parameterization favoring deeper layers. The shallower location of this layer seems to be confirmed by more recent global modeling (J. P. Montagner, personal communication, 1989).

A question which arises immediately is whether the degree 2 found in the Q maps could be an artifact due to the data processing procedure or some incorrect way of handling how lateral heterogeneities in velocity and anelasticity interact in the seismogram, overlooked in the linear theory underlying this study. We believe the data processing is not a problem. Some doubts as to the variable filtering procedure introducing distortion in the amplitudes have been discarded by going through the entire process again using raw data. We have found extremely consistent results, both for the great circle and the minor arc maps, particularly so at periods near 200 s. This procedure has also allowed us to judge the stability of our minor arc inversions when removing a number of data (10%), since a number of raw data were discarded because of too much interference between consecutive wave trains at the longest periods (for epicentral distances beyond 130°). Another potentially serious problem is the question whether the lateral variations in anelasticity could be induced by coupling effects in a laterally heterogeneous elastic model with spherically symmetric anelasticity. The magnitude of such effects for fundamental spheroidal modes have been estimated recently in the period range of interest to us [*Tsuboi and Geller*, 1989; *Lognonné*, 1989]. According to these calculations, they are unlikely to exceed 5–10% of the reference Q model, which is within the error that we have assigned to our data. We would also expect that a correlation

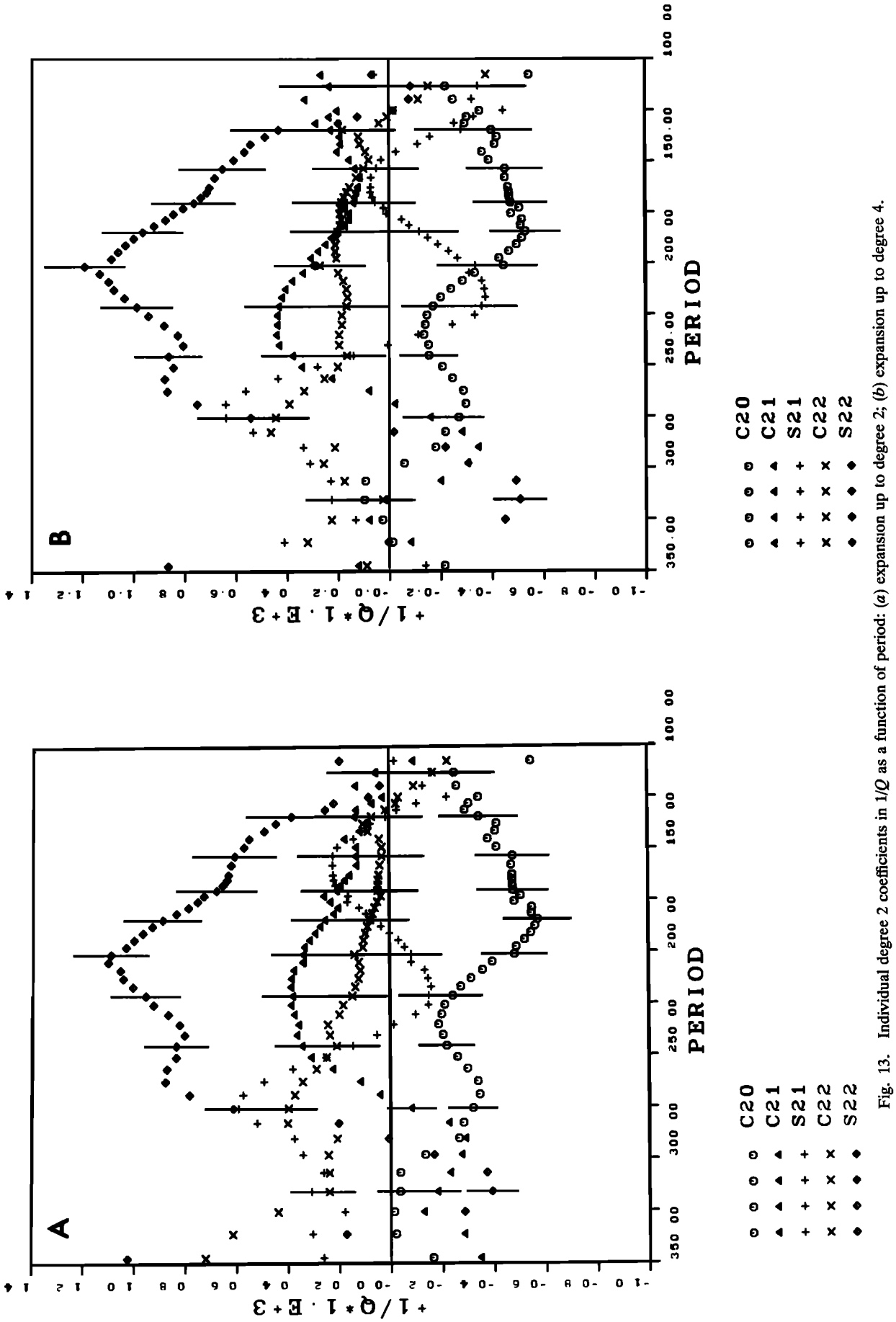

Fig. 13. Individual degree 2 coefficients in $1/Q$ as a function of period: (*a*) expansion up to degree 2; (*b*) expansion up to degree 4.

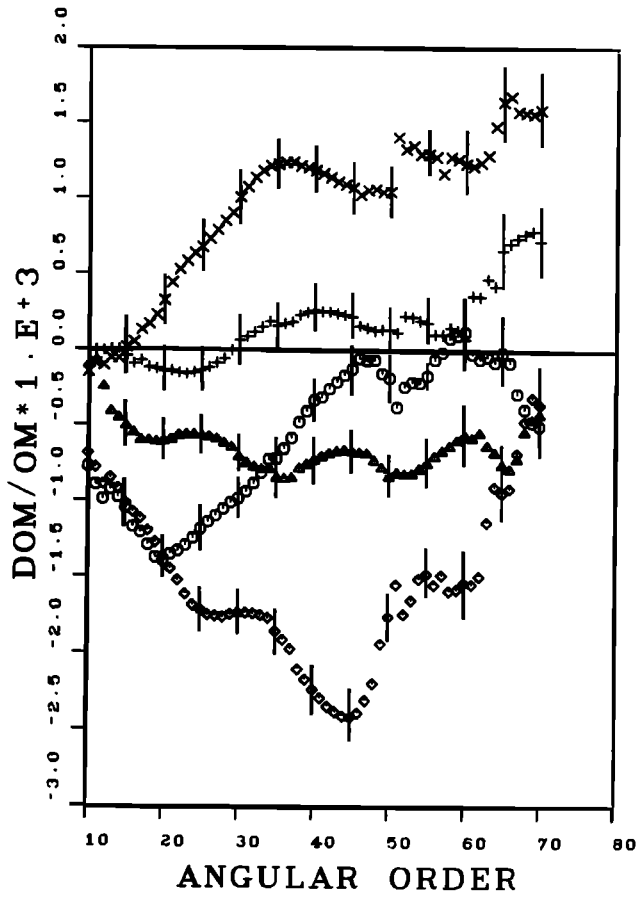

Fig. 14. Degree 2 coefficients in the expansion of relative local frequency shifts (in per mil). The symbols correspond to the same coefficients as in Figure 13. (l = 20: 347 s; l = 43: 200 s).

of this type between Q distribution and local frequency distribution should not discriminate between the S_{22} and C_{22} components.

We can now tentatively speculate as to the origin of this upper mantle degree 2 in attenuation. Intrinsic attenuation being a thermally activated process, large lateral variations in Q correlated with variations in the elastic velocities are most likely to be associated with lateral variations in temperature, even if some degree of chemical heterogeneity is present. While trying to infer actual values of lateral temperature variations in the depth range 200–500 km would be at this point rather speculative because of the little information we have on the actual physical processes causing anelasticity in the Earth's mantle, it is interesting to recall the results of numerical modelling of the temperature field inside large-scale convection cells. It is well documented that in the heart of the cells, the temperature distribution is nearly constant and varies rapidly only in the vicinity of rising and sinking plumes, causing the spectral content of the spatial distribution of the temperature to be rich in higher-order harmonics for horizontal cross sections at midheight within the cell. On the contrary [e.g., *Jarvis*, 1985], in the boundary layers and their immediate vicinity, the spectrum shifts to very low harmonics, since the temperature has smooth lateral variations within such layers. The strong degree 2 which we observe in the attenuation of long-period Rayleigh waves and which explains as much as 35% of the variance in the data at a period of 200 s is reminiscent of the thermal structure of a large-scale convective system in which we would be sampling the upper boundary layer and for which the thermal structure would be relatively well resolved by our smooth models because of its intrinsic lack of higher harmonics. This layer is located somewhat below the lithosphere and the bottom of the low-velocity zone as classically defined based on short-period measurements. We also note that both the power spectrum and the variance reduction curve in Figures 11 and 12 present a second peak at a period of about 250 s, which corresponds to a depth of maximum sensitivity in the upper mantle transition zone. Around this period, the mantle waves seem to be much less affected by focussing, and, in fact, this peak dominates the variance reduction in the data not corrected for focussing. The variance reduction is too small to allow any speculations about the origin of this peak at the present time, but further studies should permit to confirm its existence.

6. Dispersion Corrections Due to Degree 2 in Attenuation: Some Speculations and Their Implications

Let us now discuss the influence of the attenuation structure obtained on the velocity models. We will restrict our discussion to that of the robust degree 2 features, since all we can do here is to pose the problem and we are still far from being ready to propose accurate corrections to existing 3-D velocity models of the upper mantle.

Evidence from attenuation measurements spanning the frequency band from free oscillations and surface waves to long-period and short-period body waves has lead some years ago to an absorption band model for Earth whose gross features are those of a relatively constant low Q in the surface wave frequency range and down to periods of about 10 s, rapidly increasing Q between 1 and 10 s, and very high Q at higher frequencies [e.g., *Kanamori and Anderson*, 1977; *Sipkin and Jordan*, 1979; *Minster and Anderson*, 1981; *Lundquist and Cormier*, 1980; *Ulug and Berckhemer*, 1984]. While corrections of the average mantle models for dispersion due to attenuation are now routinely performed [e.g., *Anderson and Hart*, 1978], the question of how to handle the existence of lateral variations in Q within the absorption band, when comparing seismic velocity models of the upper mantle obtained at low frequencies with other geophysical data, has not yet been fully addressed. In particular, 3-D upper mantle models have been compared directly to the geoid, implicitly assuming that the conversion factor between velocities and densities does not vary laterally. While laboratory measurements have given us reliable estimates of the velocity to density relations at very high frequencies outside of the absorption band [*Birch*, 1961], there is no corresponding information at low frequencies. It seems to us that under these circumstances, the most correct procedure would presently be first to correct the upper mantle velocity models to a reference frequency outside of the absorption band before assuming a laterally constant conversion factor to other geophysical parameters such as density. We can estimate the corrections to be applied by assuming that the band limited intrinsic attenuation model with relatively constant low Q for periods above 1–10 s and much higher Q at higher frequencies is a good approximation to the real situation in the Earth. The dispersion correction due to attenuation, at angular frequency ω, is then of the form

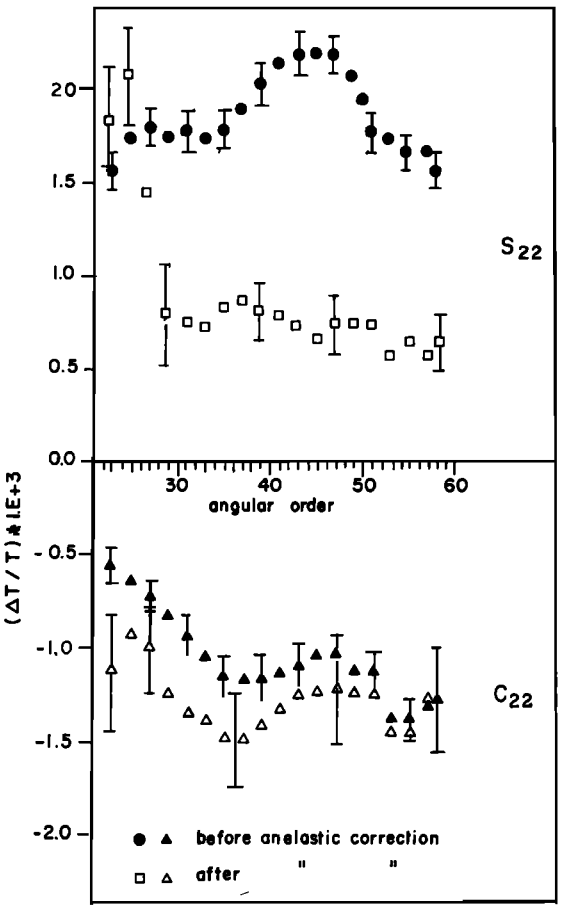

Fig. 15. $l = 2$, $m = 2$ terms of the spherical harmonics expansion of local frequency as a function of angular order before and after correction for dispersion due to attenuation, assuming a reference frequency of 1 Hz.

$$C(\omega) = C(\omega_0)\left(1 + \frac{1}{\pi Q}\ln\frac{\omega}{\omega_0}\right) \tag{6}$$

where ω_0 is a reference frequency contained within the band of constant Q. Such a model may not be quite correct for the upper mantle and is certainly oversimplified. Considerations of various power law models for $Q(\omega)$ would yield slightly different expressions for the dispersion correction [i.e., *Müller*, 1986] but not significantly alter the results of the present discussion. When lateral variations in Q are present, we must differenciate equation (6), thus obtaining corrections of the form

$$\frac{\delta C}{C} = -\frac{\delta Q}{\pi Q^2}\ln\frac{\omega}{\omega_0} \tag{7}$$

A more delicate problem is to choose a reference frequency. Since the purpose of the corrections is to be able to compare the long-period results with seismological data obtained from the analysis of short-period body waves and also laboratory measurements of physical parameters of mantle constituents made at very high frequencies, it seems appropriate to take as reference the high-frequency cutoff of the band-limited Q model, thus a frequency of about 1 Hz. As shown in Figure 15, when applying this to our degree 2 model in eigenfrequency shifts, the inferred correction in C_{22} is very small and cannot be considered as significant, given the uncertainties in the Q measurements and the choice of the exact reference period. The correction in S_{22} is much larger and leads to an overall decrease of the S_{22} term by about one half, with a disappearance of the peak at a period of about 200 s (angular orders 43–45). While the details of the variation with frequency of the corrected terms are not to be taken at face value, this exercise has two consequences: one is the change in relative amplitude of the S_{22} and C_{22} terms as measured by the ratio S_{22}/C_{22} (± -1.7 before the correction and ± -0.7 after) and the decrease by about one half of the amplitude of the 22 term as measured by the power $(C_{22}^2 + S_{22}^2)^{1/2}$. The other consequence is the net decrease in the peak in S_{22} corresponding to the 200–500 km depth range, with the remaining degree 2 distributed more uniformely with frequency and hence with depth. One implication is that corrections to the upper mantle models obtained from long-period surface wave observations or free oscillations should be applied before stripping the upper mantle contribution when studying shorter-period waves that are sensitive to lower mantle structure, or else lower mantle models can be biased, in particular by overcorrecting for the strong upper mantle degree 2. A way to check whether the proposed corrections are really necessary will be provided by the comparison of upper mantle 3-D global models obtained using mantle waves and travel times of short-period body waves. The latter should become available in the near future.

We will further note that the ratio S_{22}/C_{22} after the correction is in much better agreement with the same ratio for the observed geoid, which is of the order of -0.5 [*Reigber et al.*, 1985], leading to a better alignment of the degree 2 patterns in the observed geoid and that inferred from the upper mantle velocity maps. It is clear that the amplitudes of the corrections presented here cannot be considered at face value: a choice of a reference period of 10 s would, for example, reduce the corrections by half, and we are not certain that the law used to perform the corrections is totally realistic. The point we wish to make, however, is that careful consideration of lateral variations in upper mantle attenuation could affect the presently inferred relation between the observed geoid and the upper mantle seismic models. The upper mantle velocity models are known to be, to some extent, positively correlated to the geoid, but the preferred contributor to the geoid in the upper mantle is by far the subduction zone model [*Hager*, 1984]. This is mainly attributed to the weak response function for a dynamic earth in the upper mantle, and indeed it has been found that the longest wavelengths of the geoid can be well explained by lower mantle models [*Richards and Hager*, 1988; *Ricard*, 1985; *Hager and Richards*, 1988]. Unresolved questions still remain, however, on the existence or not of a chemical boundary at 670 km and on the viscosity increase at this depth [*Forte and Peltier*, 1987], and discriminating between different models does rely on the careful adjustment of the lower mantle response to that of the upper mantle. In particular, a better alignment of the phase of the upper mantle degree 2 velocity models as well as a decrease in the amplitude of the corresponding lateral velocity variations could help refine the comparison with the geoid and consequently improve our understanding of the rheology of the upper mantle. The present study seems to indicate that the poor agreement presently obtained between upper mantle models and the geoid may be due to excessive low velocities

obtained in regions of upwelling which are hotter, yielding high attenuation and large dispersion effects. This could perhaps also explain why the low harmonics characteristics of the convergence-divergence distribution correlate poorly with these upper mantle models [*Forte and Peltier*, 1987].

Another interesting aspect of our results is the depth extent of the zone of large-scale Q variations. Comparison of average Q models of the upper mantle inferred from long-period surface waves or free oscillations and short-period waves [*Lundquist and Cormier*, 1980; *Der et al.*, 1986; *Anderson and Given*, 1982] shows that the low Q zone for short-period waves is confined to a narrow layer not exceeding 200 km in depth, whereas that obtained from long-period waves extends down to as deep as 400 km. The degree 2 which we are seeing would then correspond to lateral variations within the long-period low-Q zone and would not be detected by short-period waves. This is in agreement with the idea [e.g., *Anderson and Given*, 1982] that different mechanisms are responsible for attenuation in the depth range 100–200 km, where partial melting may be the major factor, and in the depth range 200–400 km. If confirmed, this should put strong constraints on the mechanisms responsible for anelasticity in the upper mantle.

7. Conclusions

Global inversion of attenuation measurements of mantle Rayleigh waves indicate potentially large lateral variations in anelasticity in the upper mantle that can be related to the lateral variations in shear velocity. In particular, we have found evidence for a degree 2 pattern originating in the depth range 250–500 km and correlated with the degree 2 pattern in shear velocity observed in this depth range. This smooth component of heterogeneity is likely to be mainly of thermal origin and could be related to the topmost part of the large-scale convective system in the upper mantle.

By trying to take into account focussing effects under the assumption that higher-order asymptotics, or ray theory, work, producing linear effects that can be separated from the effects of intrinsic attenuation, this study is a first step toward correcting for nonanelastic effects in the observed amplitudes of mantle waves. Eliminating the large uncertainties in the source seismic moment by taking at least three consecutive wave trains in the analysis permits to obtain relatively accurate measurements of minor arc attenuation.

This study also shows that it is important to try to obtain 3-D anelastic models of the upper mantle with the same resolution as the presently available shear velocity models, since potentially large dispersion corrections will then have to be applied, in order to allow better comparison with short-period models as well as other geophysical parameters such as the geoid. This could lead to increased constraints on the physical properties of the mantle and their lateral variations. Present upper mantle models probably give excess low velocities in hot upwelling regions with high attenuation, shifting the low degree pattern of lateral variations with respect to that of the geoid and the subduction zone model. A better approach for future upper mantle tomographic studies will be to invert simultaneously for lateral variations in seismic velocity and attenuation. For this, we also need to make some progress in understanding the frequency dependence of anelasticity.

Acknowledgments. This study has benefitted from helpful discussions with A. Dziewonski, C. Jaupart, T. Jordan, J. P. Montagner, J. P. Poirier, and Y. Ricard. Tony Monfret contributed some of the programs used in the data analysis. The quality of the manuscript also improved following thorough reviews by two reviewers and an associate editor. The author thanks the GEOSCOPE technical team for making available the high-quality data used in this study, which was conducted under the sponsorship of INSU grant "ASP GEOSCOPE 1988". It is IPG contribution 1098.

References

Aki, K., and P. Richards, *Quantitative Seismology*, Freeman, Cooper, San Francisco, Calif., 1980.

Anderson, D. L., and J. Given, Absorption band Q model of the Earth, *J. Geophys. Res.*, *87*, 3893–3904, 1982.

Anderson, D. L., and R. S. Hart, Q of the Earth, *J. Geophys. Res.*, *83*, 5869–5882, 1978.

Birch, F., Composition of the Earth's mantle, *Geophys. J. R. Astron. Soc.*, *4*, 295–311, 1961.

Canas, J. A., and B. J. Mitchell, Lateral variation of surface wave anelastic attenuation across the Pacific, *Bull. Seismol. Soc. Am.*, *68*, 1637–1650, 1978.

Cara, M., Filtering of dispersed wavetrains, *Geophys. J. R. Astron. Soc.*, *33*, 65–80, 1973.

Davis, J. P., Variation in apparent attenuation of the Earth's normal modes due to lateral heterogeneity, *Geophys. Res. Lett.*, *12*, 141–144, 1985.

Der, Z. A., A. Lees, and V. Cormier, Frequency dependence of Q in the mantle underlying the shield areas of Eurasia, part III, The Q model, *Geophys. J. R. Astron. Soc.*, *87*, 1103–1112, 1986.

Dziewonski, A., and D. L. Anderson, Preliminary reference earth model, *Phys. Earth. Planet. Inter.*, *25*, 297–356, 1981.

Dziewonski, A. M., and R. Sailor, Comment on "The correction of great circular surface wave phase velocity measurements for the rotation and ellipticity of the Earth" by F. A. Dahlen, *J. Geophys. Res.*, *81*, 4947–4956, 1976.

Dziewonski, A. M., and J. M. Steim, Dispersion and attenuation of mantle waves through waveform inversion, *Geophys. J. R. Astron. Soc.*, *70*, 503–527, 1982.

Dziewonski, A., G. Chou, and J. Woodhouse, Determination of earthquake source parameters from waveform modelling, *J. Geophys. Res.*, *86*, 2825–2852, 1981.

Dziewonski, A. M., J. E. Franzen, and J. H. Woodhouse, Centroid moment tensor solutions for October–December 1983, *Phys. Earth Planet Inter.*, *34*, 209–219, 1984.

Dziewonski, A. M., G. Ekström, J. E. Franzen, and J. H. Woodhouse, Global seismicity of 1982 and 1983: Additional centroid moment tensor solutions for 553 earthquakes, *Phys. Earth Planet. Inter.*, *53*, 17–24, 1989.

Forte, A. M., and W. R. Peltier, Plate tectonics and aspherical Earth structure: The importance of poloidal-toroidal coupling, *J. Geophys. Res.*, *92*, 3645–3680, 1987.

Hager, B. H., Subducted slabs and the geoid: Constraints on mantle rheology and flow, *J. Geophys. Res.*, *89*, 6003–6015, 1984.

Hager, B. H., and M. Richards, Long wavelength variations in Earth's geiod: Physical models and dynamical implications, *Philos. Trans. R. Soc. London, Ser. A*, *328*, 309–327, 1989.

Jarvis, G. T., The long wavelength component of mantle convection, *Phys. Earth Planet. Inter.*, *40*, 24–42, 1985.

Jobert, N., Mantle wave propagation anomalies on laterally heterogeneous global models of the earth by Gaussian beam synthesis, *Ann. Geophys.*, *4*, 261–270, 1986.

Kanamori, H., and D. L. Anderson, Importance of physical dispersion in surface wave and free oscillation problems: Review, *Rev. Geophys.*, *15*, 105–112, 1977.

Lay, T., and H. Kanamori, Geometric effects of global alteral heterogeneity on long-period surface wave propagation, *J. Geophys. Res.*, *90*, 605–621, 1985.

Lee, W. B., and S. C. Solomon, Simultaneous inversion of surface wave phase velocity and attenuation: Rayleigh and Love waves over continental and oceanic paths, *Bull. Seismol. Soc. Am.*, *69*, 65–95, 1979.

Liu, H. P., D. L. Anderson, and H. Kanamori, Velocity dispersion due to anelazsticity: Implications for seismology and mantle composition, *Geophys. J. R. Astron. Soc.*, *47*, 41–58, 1976.

Lognonné, Ph., Modélisation des modes propres de vibration dans une Terre anélastique et hétérogéne: Théorie et observations, Ph.D. thesis, Univ. de Paris VII, 1989.

Lognonné, Ph., and B. Romanowicz, Fully coupled Earth vibrations, *Geophys. J.*, in press, 1990.

Lundquist, G., and V. Cormier, Constraints on the absorption band model of *Q*, *J. Geophys. Res.*, *85*, 5244–5256, 1980.

Masters, G., T. Jordan, P. Silver, and F. Gilbert, Aspherical Earth structure from fundamental spheroidal mode date, *Nature*, *298*, 609–613, 1982.

Mills, J., and A. Hales, Great circle Rayleigh wave attenuation and group velocity, part III, Inversion of global average group velocity and attenuation coefficients, *Phys. Earth Planet. Inter.*, *17*, 307–322, 1978.

Minster, J. B., and D. L. Anderson, A model of dislocation-controlled rheology for the mantle, *Philos. Trans. R. Soc. London*, *299*, 319–356, 1981.

Monfret, T., and B. Romanowicz, Shear velocity models of the upper mantle using GEOSCOPE data, *Eos Trans. AGU*, *69*, 1309, 1988.

Montagner, J. P., First results on the three dimensional structure of the Indian Ocean inferred from long period surface waves, *Geophys. Res. Lett.*, *13*, 315–318, 1986.

Montagner, J. P., and T. Tanimoto, Global anisotropy in the upper mantle inferred from the regionalization of phase velocities, *J. Geophys. Res.*, *95*, 4797–4819, 1990.

Müller, G., Rheological properties and velocity dispersion of a medium with power law dependence of *Q* in frequency, *J. Geophys.*, *54*, 20–29, 1986.

Nakanishi, I., Phase velocity and *Q* of mantle Rayleigh waves, *Geophys. J. R. Astron. Soc.*, *58*, 35–59, 1979*a*.

Nakanishi, I., Regional differences in the phase velocity and the quality factor *Q* of mantle Rayleigh waves, *Science*, *200*, 1379–1381, 1979*b*.

Nataf, H.-C., I. Nakanishi, and D. L. Anderson, Measurements of mantle wave velocities and inversion for alteral heterogeneities and anisotropy, 3, Inversion, *J. Geophys. Res.*, *91*, 7261–7307, 1986.

Park, J., Aasymptotic coupled mode expressions for multiplet amplitude anomalies and frequency shifts on an aspherical earth, *Geophys. J. R. Astron. Soc.*, *90*, 129–164, 1987.

Reigber, C., G. Balmino, H. Miller, W. Bosch, and B. Moynot, GRIM gravity model improvement using LAGEOS (GRIM3-L1), *J. Geophys. Res.*, *90*, 9285–9299, 1985.

Ricard, Y., Dynamique interne de la Terre et observations gravimétriques, Ph.D. thesis, Univ. Paris-Sud, Orsay, 1986.

Richards, M., and B. H. Hager, The Earth's geoid and the large scale structure of mantle convection, in *The Physics of the Planets*, edited by S. K. Runcorn, pp. 247–271, John Wiley, New York, 1988.

Romanowicz, B., Multiplet-multiplet coupling due to lateral heterogeneity: Asymptotic effects on the amplitude and frequency of the Earth's normal modes, *Geophys. J. R. Astron. Soc.*, *90*, 75–100, 1987.

Romanowicz, B., and Ph. Guillemant, An experiment in the retrieval of depth and source mechanism of large earthquakes using very long period Rayleigh wave data, *Bull. Seismol. Soc. Am.*, *74*, 417–437, 1984.

Romanowicz B., and T. Monfret, Source process times and depths of large earthquakes by moment tesnor inversion of mantle wave data and the effect of lateral heterogeneity, *Ann. Geophys.*, *4*, 271–283, 1986.

Romanowicz, B., M. Cara, J. F. Fels, and D. Rouland, GEOSCOPE: A French initiative in long period three component seismic networks, *Eos Trans AGU*, *60*, 753–754, 1984.

Romanowicz, B., G. Roult, and T. Kohl, The upper mantle degree two pattern: Constraints from GEOSCOPE fundamental spheroidal mode eigenfrequency and attenuation measurements, *Geophys. Res. Lett.*, *14*, 1219–1222, 1987.

Romanowicz, B., G. Ekström, and Ph. Lognonné, On how to handle focussing effects in long period Rayleigh wave attenuation measurements (abstract), *Eos Trans. AGU*, *70*, 1186, 1989.

Roult, G., The effect of young oceanic regions on frequencies and damping of free oscillations of the Earth, *J. Geophys.*, *51*, 38–43, 1982.

Roult, G., and B. Romanowicz, Very long period data from the GEOSCOPE network: Preminimary results on great circle averages of fundamental and higher Rayleigh and Love modes, *Bull. Seismol. Soc. Am.*, *74*, 2221–2243, 1984.

Roult, G., B. Romanowicz, and J. P. Montagner, 3D upper mantle shear velocity and attenuation from fundamental mode free oscillation data, *Geophys. J.*, *101*, 61–80, 1990.

Sailor, R., and A. M. Dziewonski, Measurements and interpretation of normal mode attenuation, *Geophys. J. R. Astron. Soc.*, *53*, 559–581, 1978.

Sipkin, S. A., Estimation of earthquake source parameters by the inversion of waveform data: synthetic waveforms, *Phys. Earth Planet. Inter.*, *30*, 242–259, 1982.

Sipkin, S. A., and T. H. Jordan, Frequency dependence of Q_{ScS}, *Bull. Seismol. Soc. Am.*, *69*, 1055–1079, 1979.

Sipkin, S. A., and T. H. Jordan, Regional variation of *QScS*, *Bull. Seismol. Soc. Am.*, *70*, 1071–1102, 1980.

Smith, M. F., and G. Masters, Aspherical structure constraints from free oscillation frequency and attenuation measurements, *J. Geophys. Res.*, *94*, 1953–1976, 1989.

Tanimoto, T., The Backus Gilbert approach to the 3D structure in the upper mantle, II, *SH* and *SV* velocity, *Geophys. J. R. Astron. Soc.*, *84*, 49–69, 1986.

Tarantola, A., and B. Valette, Generalized nonlinear inverse problems solved using the least squares criterion, *Rev. Geophys.*, *20*, 219–232, 1982.

Tsuboi, S., and R. J. Geller, Coupling between the multiplets of laterally heterogeneous Earth models, *Geophys. J.*, *96*, 371–379, 1989.

Ulug, A., and H. Berckhemer, Frequency dependence of *Q* of seismic body waves, *J. Geophys.*, *56*, 9–19, 1984.

Woodhouse, J. H., and A. M. Dziewonski, Mapping the upper mantle: Three-dimensional modeling of Earth structure by inversion of seismic waveforms, *J. Geophys. Res.*, *89*, 5953–5986, 1984.

Woodhouse, J. H., and Y. Wong, Amplitude, phase and path anomalies of mantle waves, *Geophys. J. R. Astron. Soc.*, *87*, 753–773, 1986.

Yacoub, N. K., and B. J. Mitchell, Attenuation of Rayleigh wave amplitudes across Eurasia, *Bull. Seismol. Soc. Am.*, *67*, 751–769, 1977.

B. Romanowicz, Laboratoire de Sismologie, Institut de Physique du Globe, 4 Place Jussieu, Tour 14, 75252 Paris Cedex 05, France.

(Received March 3, 1989;
revised November 20, 1989;
accepted October 25, 1989.)